UNIVERSITÀ DEGLI STUDI DI PALERMO

FACOLTA' DI AGRARIA
DIPARTIMENTO DI SCIENZE AGRARIE E FORESTALI

Dottorato di Ricerca in
"Tecnologie per la Sostenibilità ed il Risanamento Ambientale"
Ciclo XXIV
Triennio 2011-2013
SSD: AGR/13 – Chimica Agraria

STUDY OF CHEMICAL-PHYSICAL PROPERTIES IN INDUSTRIAL BIOCHAR

TESI DI
Valentina Marsala

TUTOR
Prof. Pellegrino Conte

CO-TUTOR
Prof. Giuseppe Alonzo

COORDINATORE DEL DOTTORATO
Prof. Sebastiano Calvo

AKNOWLEDGEMENT

I would like to thank my supervisor Prof. Conte for his expertise, his knowledge his patience and his assistance during my graduate experience. I am very grateful to Prof. Alonzo for his enthusiastic approach to new projects.

A special thanks to the coordinator of the PhD course, Prof. Calvo for his availability.

I would like to thank also Prof. Palazzolo and Dr. Panno and Dr. Laudicina for their kind collaboration during my work activity. Thanks to Claudio for his scientific support and his kindness.

I would express my gratitude to Dr. Berns for her knowledge and for the excellent working conditions she provided during my experience abroad. A special thanks also to Prof. Pekar who has been an attentive supervisor during my stay in his laboratory in Brno.

Thanks to Dr. Kucerik for his advices and his kind collaboration.

I would like to tank Professor Palmisano, Dr. Loddo, and Dr. Parrino for their collaboration and for the constructive scientific discussions.

A Special thanks to Dr. Pozzi and to Dr. Valagussa for their knowledge and their comments.

I am very grateful to whole my family for their support and encouragement.

Finally, a very special thanks to my friends, and colleagues. To Giulia, Farid, Gabriella, Anna, Rita, Melina, Loredana, Vincenzo, Lucio I have really enjoyed the nice time spent together and I appreciated their support in hard moments.

INTRODUCTION

In literature there are many definition to describe biochar. Nowadays the most used in the scientific community is the one suggested by Lehman and Joseph in 2009: “biochar is charred organic matter, produced with the intent to apply to soil in a deliberate manner with the intent to improve soil properties”. The term distinguishes application of biochar from other carbonaceous material used as a fuel for heat or for different technological applications. An other interesting property is its stability. Its recalcitrance to degradation, in fact, suggested to use it to store carbon into soil and to reduce its release in atmosphere as CO_2. This application it could be a contribute to reduce greenhouse effect therefore global warming.

Biochar is produced by thermal degradation of biomass under oxygen-limited conditions. Its utilization as a soil amendment is an actual topic discussed by several authors because it could be a very important role in soil management, and in energetic biomass conversion.

In the last 14 years published papers on biochar increased exponentially, to confirm strong interest on this topic (fig.1).

Use of biomass as an energy source in substitution of traditional fossil fuel is a possible and viable alternative in the perspective of climate mitigation strategies. Potential increment of biochar production in future is predictable.

Nowadays, there are at least two barriers to technology implementation, the lack of commercial biochar available to farmers and most importantly, legislative barriers that prevent it being applied to land. The lack of inclusion of biochar in current agricultural policy is due to the major uncertainty surrounding the long term behavior of biochar, its potential negative impacts on soil quality, and the fact that it

cannot easily be removed from soil after addition. (D.L. Jones et al., 2012). Some authors suggest attention in a possible negative outcomes, as a possible addiction of xenobiotics compounds as polyaromatic hydrocarbons into the soil or a possible prevention in the action of pre-emergent herbicides (D.L. Jones et al., 2012)

A deep knowledge on this material has a paramount importance before to address its use in environmental application. In fact Biochar properties depend on original biomass and conditions of thermal treatment.

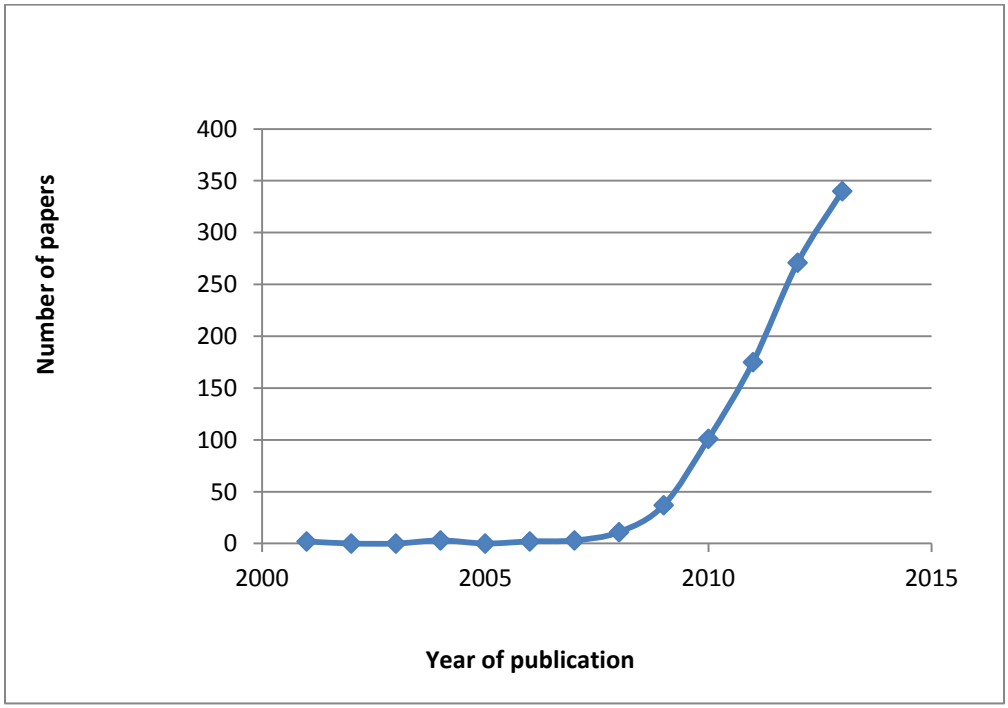

Fig. 1 increment of number of papers about biochar from2000 to 2013 (Scopus database)

References

D.L. Jones, J. Rousk, G. Edwards-Jones, T.H. DeLuca, D.V. Murphy Biochar-mediated changes in soil quality and plant growth in a three year field trial Soil Biology & Biochemistry 45 (2012) 113e124

Lehmann J, Joseph S (2009) Biochar for environmental management:an introduction. In: Lehmann J, Joseph S (eds) Biochar for environmental management: science and technology. Earthscan, LondonLehman and Joseph in 2009

1. AIM OF THE THESIS

Because of interest to use biochar as amendment in soil, a carachterization of this carbonaceous material has a relevant importance to avoid a detriment of soil properties, and to address biochar utilization in the best way for environmental application. Industrial biochar is considered a by-product of the thermochemical conversion of biomass for energy production, and it treated as waste.

In particular the aim of this study is to understand chemical-physical properties of industrial biochar, derived from a gasification process.

This study adds some important informations on actual knowledge on biochar properties and on water interaction with biochar surface.

The topic is the evaluation of chemical-physical properties of this material that it can be used as an important source from the economic, social and environmental point of view.

Attention was focused on biochar surface properties and on porosity distribution of the carbonaceous material, two important parameters that influence soil properties and its interaction with water, plants and soil biota.

During research activity biochars derived from three different biomasses after gasification at 1200 °C. after routine chemical characterization, samples have been analysed by applying ^{13}C CPMAS NMR spectroscopy, in order to study their chemical composition and then by applying FFC NMR Relaxometry to investigate water dynamic on biochar surface. Briefly, results showed that biochars have a different interaction with water because of their pore size distributions. FFC NMR

Relaxometry allows to understand drainage properties of samples because permits to evaluate water dynamic depending on porosity.

The FFC NMR Relaxometry was applied analyzing biochar sample at different temperature to avaluate deeply the mechanism of water dynamics on biochar surface.

Results suggested that water molecules are bound to the solid surface of carbon through nonconventional bonds.

In order to study potential of biochar in environmental remediation, studies of its possible use in addiction to Titanium dioxide have started. This is a low cost compound, applied in several sector and it has a big importance also in photocatalysis for pollutant abatement. The aim of the research is to evaluate the effectiveness of doped carbon to develop a convenient and efficient technology to treatment of polluted water.

Hence the necessity to study water interaction on the surface of different titanium dioxide polymorphs. The thesis reported first results of a preliminary study on this topic.

.

2. BIOENERGY SOURCES AS A POSSIBLE AND VIABLE ALTERNATIVE TO FOSSIL FUELS IN THE PERSPECTIVE OF CLIMATE MITIGATION STRATEGIES

In recent years climate changes became one of the most important challenge for humanity. Emissions from fossil fuels are the largest contributor to the anthropogenic greenhouse effect, so a reduction in fossil-energy use is a clear priority. At the same time, however, since 1992 energy consumption world wide has steadily increased, and it will increase by 2% per year until 2020 (Alonzo, 2006).

Fossil fuels are considered to be non-renewable sources of energy considering the rate of their formation (millions of years) and consumption. In addition, burning fossil fuels releases net carbon dioxide (CO_2) to the atmosphere (Zhang et al., 2010).

The increasing availability of biomass, combined with the recent development of technologies to use it efficiently and with low levels of emissions, promise to make biomass an increasingly attractive fuel option. Biomass, in contrast to fossil fuels, has a unique potential for making a positive environmental impact (Quaak et al., 1999). Biomass is considered a carbon neutral fuel because when biomass is used in combustion process, releases CO_2 that the plants have absorbed from the atmosphere through photosynthesis process (Basu, 2010).

In addition, the lower emission of environmentally detrimental gases, such as sulphur dioxide (SO_2) and nitrogen oxides (NOx), during the combustion of biomass also plays a positive role in reducing global acid rain formation. Biomass includes a wide range of organic materials, which are generally composed of cellulose, hemicellulose, lignin, lipids, proteins, simple sugars and starches. Among these

compounds, cellulose, hemicellulose, and lignin are the three main constituents. Biomass also contains inorganic constituents and a fraction of water. As for the elementary composition, carbon (51 wt.%) and oxygen (42 wt.%) together contribute to over 90% of the dry weight of a typical biomass. In addition, there are trace amounts of hydrogen (5 wt.%), nitrogen (0.9 wt.%) and chlorine (0.01–2 wt.%). Wood, energy crops, as well as agricultural and forest residues, which are the main renewable energy sources, are typical examples of biomass. Moreover, food processing wastes, sewage sludge, and the organic components of municipal solid waste (MSW) and pulping by-products (e.g., black liquor) can also be considered biomass (Zhang et al., 2010; IEA,2007).

One of the most important biomass fuels is wood. But wood is often too valuable to burn, and woodworking industries are able to make better use of trees by processing them into construction materials. True residues such as bark, sawdust, and misshapen or odd-sized pieces are frequently more economic to use as fuel.

Many agricultural residues can be used as fuels. In addition, forestry and landscape conservation activities generate biomass such as thinnings and verge grass. Using these biomass residues as fuels may solve the environmental problem of how to dispose of them. Moreover, the potential for using residues as a source of energy may create new incentives to grow crops that are now only marginally profitable.

Cultivation of biomass specifically for direct use as a fuel-known as energy cropping-may create new incentives for the agricultural sector, particularly in countries that suffer from overproduction of crops (Quaak et al., 1999).

In this scenario development of clean technologies using renewable resources as biomasses to produce energy on several forms, is very attractive. Probably this is one of the most important answer to energy request all over the world that allows at the same time to contrast climate changes. In particular biochar production, when combined with energy production, it is a clean energy technology that reduces emissions as well as sequesters carbon (J. Lehmann, 2007).

References:

Alonzo G, Aiello P L'uso di energia da fonti rinnovabili Regione Siciliana (2006).

Basu P. (2010) Biomass gasification and pyrolysis: practical design and theory. Academic Press, New York, ISBN: 9780123749888.

IEA (International Energy Agency). Bioenergy project development &biomass supply, <http://www.iea.org/textbase/nppdf/free/2007/biomass.pd

Lehmann, J., 2007. A handful of carbon. Nature 447, 143e144.

Quaak P,. Knoef H., Stassen H. Energy from Biomass A Review of Combustion and Gasification Technologies 1999 WORLD BANK TECHNICAL PAPER NO. 422 Energy Series

Zhang L., Xu C., Champagne P. Overview of recent advances in thermo-chemical conversion of biomass Energy Conversion and Management 51 (2010) 969–982

3. BIOMASS CONVERSION

Bioenergy can be converted from biomass via two main types of processes: thermo-chemical and bio-chemical/biological processes (Zhang et al., 2010)

The latter includes three main routes:

Digestion (aerobic and anaerobic)

Fermentation

Enzymatic or acid hydrolysis

In these processes biomass molecules are broken into smaller molecules by bacteria or enzymes, this process is usually less efficient and much slower, but does not require much external energy (Basu, 2010).

Biological degradation of organic matter (OM) under anaerobic conditions originates different products, the most abundant of which are methane, used to produce energy and heat, and carbon dioxide (Tambone et al., 2013).

Thermo-chemical conversion processes mainly include direct combustion, pyrolysis, gasification, and liquefaction. The stored energy within biomass could be released directly as heat via combustion/co-firing, or could be transformed into solid (e.g., charcoal), liquid (e.g., bio-oils), or gaseous (e.g., synthetic gas and short for syngas) fuels via pyrolysis, liquefaction, or gasification with various utilization purposes (Zhang et al., 2010).

Each type of biomass has specific properties that determine its performance as a fuel in combustion or gasification devices or both. The most important properties relating to the thermal conversion of biomass are as follows:

* Moisture content

* Ash content
* Volatile matter content
* Elemental composition
* Heating value
* Bulk density

(Quaak et al., 1999)

3.1 Biochar production by Thermo-chemical conversion

Carbonized organic matter can have fundamentally different physical and chemical properties depending on the thermal treatment condition and on the original biomass. Several different technologies are available, each one more convenient to the intended purpose: torrefaction, slow pyrolysis, intermediate pyrolysis, fast pyrolysis, gasification, hydrothermal carbonization (htc), or flash carbonization. Research on torrefied material as soil amendment has started only recently. On the contrary several publication to assess the value of charcoal as soil amendment, are available (Meyer et al.,2011).

Carbonization of biomass residue and waste materials has great potential to become an environmentally sound conversion process for the production of a wide variety of products. However, there are many aspects that require additional research. Filling the current research gaps is necessary before the process can be designed and exploited to produce char for specifically intended applications (Libra et al., 2011). Also manure from animal farming can be converted into biochar.

Conversion of poultry litter in biochar using pyrolysis could be a safer and more effective alternative to use this resource in agriculture but more investigation is necessary (Chan et al.,2008).

Both the temperature and particle size have significant effects on char yield. At higher temperature, the heat flux is higher. The size of the particles affects the heating rate. The heat flux and the heating rate are higher in small particles than in large particles. The higher heating rate favors a decrease of the char yield (Demirbas, 2004; Manyà, 2012). the heating rate is mainly affected by the radiation temperature and the particle size. Moreover, the density of the biomass particles has a relevant influence. Compared to the other parameters, the moisture content shows only small influences (Mehrabian et al., 2010). A number of factors may have contributed to the increasing char yield due to the increase of biomass particle size. Firstly, the intra-particle mass transfer resistance is much higher in the bigger particle than smaller one. During pyrolysis the tar concentration in the char matrix increases with increasing particle size and the large tar concentration implies extensive recombination of tarry compounds on the internal surface of the char, resulting in reduced weight loss of char. Secondly, the temperature distribution from the surface to the centre of the particle is not the same during pyrolysis of bigger particles. The centre part of a particle is always experienced lower temperature than that of the outer surface during heating up. This temperature gradient is generated in fact by two reasons. The first reason is the consumption of heat by endothermic initial pyrolysis process and the second reason is the lower thermal conductivity of wood particle. Therefore, the heating rate of the central mass is much slower than that of the outer mass. It seems that the devolatilization of central mass is slower,

leading to the recombination of volatiles. Another important reason is the ‘‘self-gasification” of char by volatiles. As the biomass particles were fed continuously into the reactor, the species in the volatiles such as H_2O and CO_2 would react with char to result in the gasification of char. Clearly, this would be a function of the extent of volatile–char interactions and it is more significant for smaller particles of biomass. As a result, the char yield increased with increasing biomass particle size obtained similar results in their study to examine the effect of temperature and particle size of various biomasses on biochar yield and reactivity. With the increase of biomass particles the biochar yield was increased (Asadullah et al., 2010). An increase of peak temperature seems to lead to the generation of biochars with higher aromatic character and fixed carbon and higher porosity. Further studies analyzing the effect of pyrolysis peak temperature on both biochar stability and nutrient retention (CEC) are required to confirm this preliminary trend (Manyà, 2012).

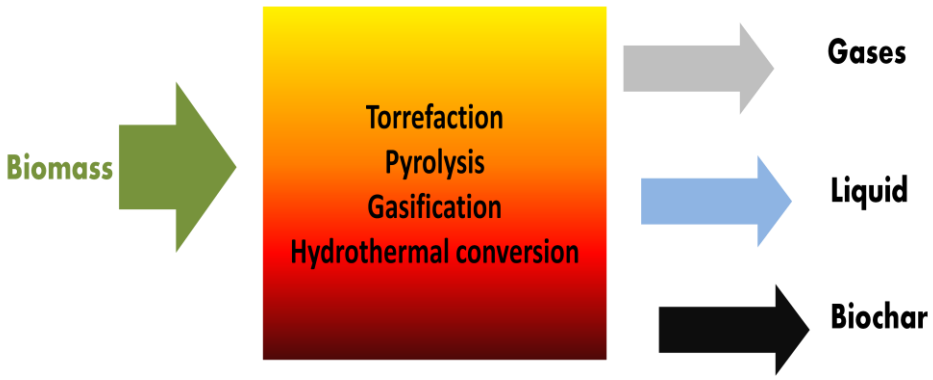

Fig. 2 Thermo-chemical conversion

3.1.1 Torrefaction

Torrefaction improves the solid fuel properties of biomass. It is a mild temperature pyrolysis process that removes moisture and a proportion of the volatile content and leaves a dry, partially carbonised solid (Bridgeman et al., 2010). Torrefaction is considered to be very attractive due to its advantage in improved fuel volumetric energy density as well as increased grindability. Torrefaction is usually performed in inert atmosphere at temperature below 300 $^{\circ}$C which aims to remove mostly the major hemicellulose contents from biomass structure. During torrefaction, H_2O and acid compounds were found to be the main condensable volatile products while CO_2 and CO were the major non-condensable gaseous products formation (Wannapeera et al., 2011). As a result, both the O/C and the H/C ratios of the biomass decrease. Increment of the O/C ratio it is an advantage because it improves biomass gasification efficiency.

This technology offers several advantages as reduction of power requirements for size reduction, and handling improvement. It offers cleaner-burning fuel with little acid in the smoke. A fuel gas that has an enhanced heating value may be obtained through gasification.

In addiction torrefied wood absorbs less moisture when stored and one can produce superior-quality biomass pellets with higher volumetric energy density (Basu, 2010).

3.1.2 Pyrolysis

The main process for char production with significant yields is the dry pyrolysis process. It has been used by mankind for millennia to produce charcoal and tar-like substances, although it can be operated to produce multiple products (e.g., oil and gas) beside char. The so called ‘dry distillation’ of wood also yields methanol, acetic acid, acetone and many more base chemicals. Moderate heating rates with long residence times (slow or intermediate pyrolysis yield high amounts of gases and vapors (30–35%) and approximately 20–40% as char. In industrial applications, these processes are operated in closed kilns where the non condensable gases are used to fire the reactors (Libra et al., 2011).

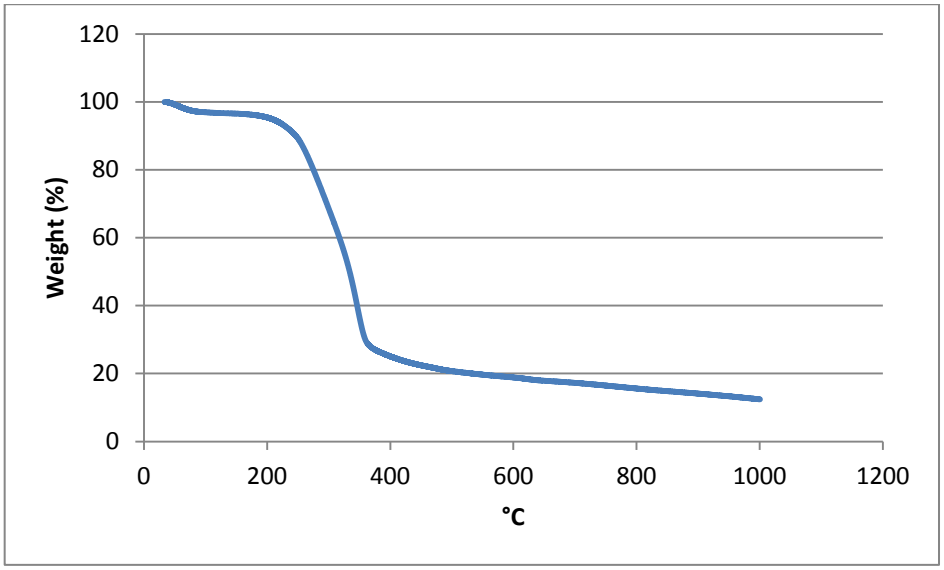

Fig. 3 Thermograms of oak sawdust in Nitrogen atmosphere

Different steps characterize pyrolysis process. Graph above shows thermograms of oak sawdust heated from room temperature to 1000°C in nitrogen atmosphere. Each step in the thermograms indicates different phases in the process. Around 100°C free moisture and some loosely bound water is released (Drying). At 100-300°C exothermic dehydration takes place with the release of water and low-molecular-weight gases (Initial stage). The primary pyrolysis takes place in the temperature range of 200-600°C. During this phase large molecules of biomass particles decompose into char (primary char), condensable gases (vapors and precursor of the liquid yeld), and condensable gases. The final stage of pyrolysis (300-900°C) involves secondary cracking of volatiles into char and non condensable gases. Higher temperature favors production of hydrogen, above 900°C the hydrogen yield increases (Basu 2010).

3.1.3 Gasification

Gasification is a thermal conversion process that occurs at high temperature in presence of an oxidizing atmosphere. The addition of air, oxygen, steam or carbon dioxide or a mixtures of both, is necessary to rearrange the molecular structure of the feedstock in order to convert the solid feedstock into gases or liquids (Basu, 2010). The product gases, a mixture of mainly H_2, CO, CO_2 and CH_4, can be used directly as a fuel or as a synthesis gas (syngas) in downstream catalytic conversion processes to generate synthetic natural gas (SNG), methanol, Fischer-Tropsch fuels and many more products. Gasification is generally operated in a continuous mode and maximized to produce gas, with yields of approximately 85%; only a small amount of char is produced (Libra et al., 2011). Most papers focus on pyrolysis technologies, less information is available on gasification processes. Publications on gasification processes often do not take into account the potential suitability of the char as a product for soil improvement (Meyer et al.,2011).

Gasification is a complex process that involves several chemical reaction, during several steps as:

Drying; pyrolysis; partial combustion of some gases, vapors, and char; gasification of decomposition products.

Drying is necessary for the production of a fuel gas with a high heating value, for this reason biomass should have a moisture content around 10-20%. During pyrolysis process hydrocarbon molecules undergo a thermal breakdown into smaller molecules. The subsequent gasification step includes several chemical reaction

among hydrocarbons in fuel, steam, CO_2, O_2, H_2 in the reactor, as well as chemical reactions among the evolved gases. (Basu, 2010)

The reactions involved in the gasification step are the follows:

$C + CO_2 \rightarrow 2\ CO$

$C + H_2O \rightarrow CO + H_2$

$CO + H_2O \rightarrow CO_2 + H_2$

$CO_2 + H_2 \rightarrow CO + H_2O$

$C + 2\ H_2 \rightarrow CH_4$

(De Pasquale et al. 2011)

Actually several different gasification technologies are available. Each one offer advantages and different yelds of product. Briefly here are listed the most common types.

Usually gasifiers are classified in three principal types on the basis of gas-solid contacting mode and gasifying medium:

-FIXED OR MOVING BED.

In this case biomass is supported on a grate and it moves down in the gasifier as a plug. This kind of gasifier is characterized for its small dimension and low cost. On the basis of the direction and the imput of the gasification medium (air, oxygen or steam) three kind of fixed or moving bed gasifiers can be distinguished: Updraft, downdraft and crossdraft gasifiers. In the first, oxidant medium moves upward in countercurrent mode of solid fuel that moves downward. The product gas leaves the gasifier from the top.

In the downdraft gasifier air enters in at a certain height below the top, following the same direction of biomass. The product gases in this case move downward through the high temperature zone of hot ash, where condensable fraction of gas product finds conditions for cracking. For this reason this type of gasifier produces a low tar fraction. In the crossdraft biomass enters in from the top while air from a side of gasifier. In this case gas product leaves from the opposite side of the entry point of the oxidant medium. This kind of gasifier has a low tar production, and is used in small-scale biomass unit. (Basu, 2010)

-FLUIDIZED-BED GASIFIER

Their most important feature is the very good gas- solid mixing and temperature uniformity. Granular biomass is fed into a fluidized bed, made of a granular solid kept in a fluidized state by the flow of the gasifying medium through it.

In the bubbling fluidized-bed gasifier is the one most common for biomass gasification, but they are suitable for medium – size units.

The circulating fluidized-bed gasifier is very suitable for biomass gasification because of the long gas residence time needed in the reactor.

3.1.4 Hydrothermal processes

In hydrothermal processes, the solid material is surrounded by water during the reaction, which is kept in a liquid state by allowing the pressure to rise with the steam pressure in (high)-pressure reactors. As in dry pyrolysis, reaction temperature (and pressure) determines the product distribution. With process temperatures of up

to 220°C and corresponding pressures up to approximately 20 bar, very little gas (1–5%) is generated, and most organics remain as or are transformed into solids. At higher temperatures, up to approximately 400°C, and with the use of catalysts, more liquid hydrocarbons are formed and more gas is produced (Libra et al., 2011).

Hydrothermal treatment offers significant advantages for biomass conversion including the lack of an energy-extensive drying process, high conversion efficiency and relatively low operation temperature among thermal methods (Liu et al.,2013).

REACTION CONDITIONS AND PRODUCT FOR THERMOCHAMICAL CONVERSION PROCESSES				
PROCESS	TEMPERATURE; VAPOR RESIDENCE TIME	PRODUCT DISTRIBUTION (WEIGHT%)		
		CHAR	TAR	GAS
PYROLYSIS	400-500°C; FEW SECONDS - WEEK	35-12	75-30	35-13
GASIFICATION	800°C - 10-20 S	10	5	85
HYDROTHERMAL CONVERSION	180-250°C; NO VAPOR RESIDENCE TIME, 1-12H PROCESSING TIME	50-80	5-20	2-5

Tab. 1 (Libra et al., 2011, modified)

References:

Asadullah M., Zhang S., Min Z., Yimsiri P., Li C. L. Effects of biomass char structure on its gasification reactivity Bioresource Technology 101 (2010) 7935–7943

Basu P. (2010) Biomass gasification and pyrolysis: practical design and theory. Academic Press, New York, ISBN: 9780123749888

Bridgeman T.G., Jones J.M., Williams A.,Waldron D.J. An investigation of the grindability of two torrefied energy crops Fuel 89 (2010) 3911–3918

Chan K.YVan Zwieten., L., Meszaros I., Downie A., and Joseph S. Using poultry litter biochars as soil amendments Australian Journal of Soil Research, 2008, 46, 437-444

Demirbas A. Effects of temperature and particle size on bio-char yield from pyrolysis of agricultural residues J. Anal. Appl. Pyrolysis 72 (2004) 243–248

Libra J.A., Ro K.S., Kammann C., Funke A., Berge N.D., Neubauer Y., Titirici M.M., Fühner C., Bens O., Kern J. Emmerich K.H. Hydrothermal carbonization of biomass residuals: a comparative review of the chemistry, processes and applications of wet and dry pyrolysis Biofuels (2011) 2(1), 89–124Liu et al.,2013).

Joan J. Manya Pyrolysis for Biochar Purposes: A Review to Establish Current Knowledge Gaps and Research Needs dx.doi.org/10.1021/es301029g | Environ. Sci. Technol. 2012, 46, 7939−7954

Mehrabian R., Scharler R., Obernberger I. Effects of pyrolysis conditions on the heating rate in biomass particles and applicability of TGA kinetic parameters in particle thermal conversion modeling Fuel 93 (2012) 567–575

Sebastian Meyer, Bruno Glaser, and Peter Quicker Technical, Economical, and Climate-Related Aspects of Biochar Production Technologies: A Literature Review dx.doi.org/10.1021/es201792c | Environ. Sci. Technol. 2011, 45, 9473–9483.Meyer et al.,2011)

Quaak P,. Knoef H., Stassen H. Energy from Biomass A Review of Combustion and Gasification Technologies 1999 WORLD BANK TECHNICAL PAPER NO. 422 Energy Series

Tambone F., Adani F., Gigliotti G., Volpe D., Claudio Fabbri, Provenzano M.R. Organic matter characterization during the anaerobic digestion of different biomasses by means of CPMAS 13C NMR spectroscopy Biomass and Bioenergy 48 (2013) 111e120Tambone et al., 2013).

Wannapeera J., Fungtammasan B., Worasuwannarak N.Effects of temperature and holding time during torrefaction on the pyrolysis behaviors of woody biomass Journal of Analytical and Applied Pyrolysis 92 (2011) 99–105

Zhang L., Xu C., Champagne P. Overview of recent advances in thermo-chemical conversion of biomass Energy Conversion and Management 51 (2010) 969–982

4. BIOCHAR PROPERTIES

Biochar is commonly defined as charred organic matter, produced with the intent to deliberately apply to soils to sequester carbon and improve soil properties (based on: Lehmann and Joseph, 2009).

Biochar production contribute to promote to use biomass feedstocks to produce energy and at the same time to sequester carbon reducing CO2 emissions in atmosphere.

The only difference between biochar and charcoal is in its utilitarian intention; charcoal is produced for other reasons (e.g. heating, barbeque, etc.) than biochar. In a physicochemical sense, biochar and charcoal are essentially the same material.(Verheijen et al.,2009)

As with other mitigation technologies, biochar needs to be evaluated in terms of three basic criteria: effectiveness, efficiency and equity. Projects in developing regions offer the highest opportunities for greenhouse gas abatement using biochar because a large number of low-tech projects can be set up within each region. These projects use a cheap technology and resources already in being used by billions of people today whereas the projects in developed regions require large amounts of start-up capital and running costs for a new technology. (Pratt et al.,2010). Biochar can be produced by applying several technologies as mentioned above. In several papers results did not show an improvement of plant growth after the addition of carbonized material from torrefaction, hydrothermal carbonization, and flash carbonization (Meyer et al., 2011).

4.1. Structure

Charred biomass has a typical structure characterized by the presence of condensed (fused) aromatic rings. Dimension of grapheme sheets gets larger as the extent of thermal alteration increases, and the structure tends to form stacks with disordered packing.

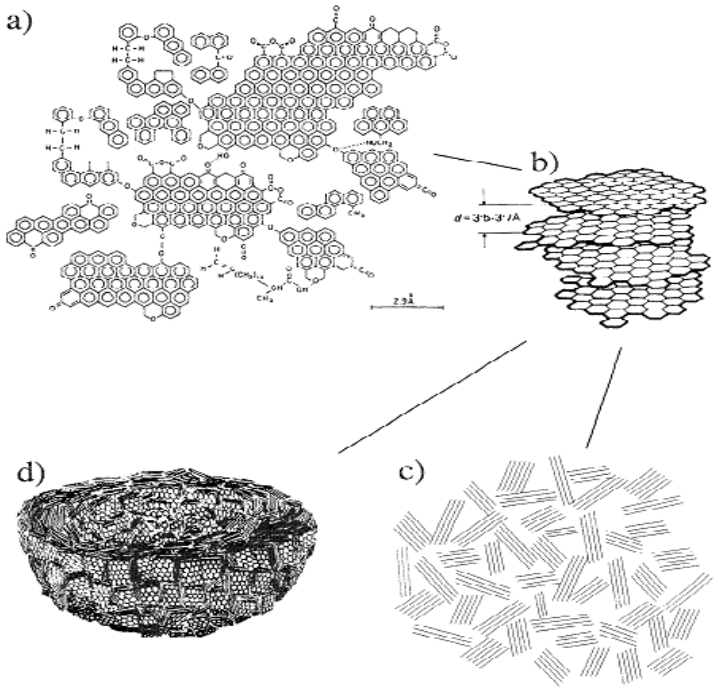

Fig. 4 Black Carbon molecular structure (Schmidt and Noak, 2000. Reproduced with permission from Wiley).

Functional groups contain mainly oxygen (O) or hydrogen (H), and the degree of functionalization is reflected in the molar ratios O/C and H/C. The number of functional groups, important for biological degradability, is strongly dependent on original biomass and on thermal process. It decreases continously from unaltered biomass to increasingly thermally-altered structures. (Large O/C and H/C ratios

indicate the presence of many functional groups, whereas smaller ratios are typical for more condensed structures, with ratios close to 0.0 typical for almost pure carbon (Preston et al., 2006).

By convention, thermally altered natural organic matter is assumed as charcoal with an O/C ratio of less than 0.6 as reported in Glaser (2006).

The O:C molar ratio is a more reliable predictor of overall stability of biochar in soils might be. This ratio is the net result of all of the multiple parameters during the production, cooling and storage of the biochar. biochar with an O:C molar ratio of less than 0.2 are typically the most stable, possessing an estimated half-life of more than 1000 years; biochar with an O:C ratio of 0.2–0.6 have intermediate half-lives (100–1000 years); and, finally biochar with an O:C ratio of greater than 0.6 possess a half-life in the order of over 100 years (Spokas, 2010).

This property can allow biochar to act as a carbon sink (Sohi, S.; et al.,2009).

It was also demonstrated that concentration of Nitrogen compounds in original biomass influences recalcitrance to thermal degradation. Although N-rich material produced more char with greater heat resistance than cellulose-rich plant residue (Knicker, 2010).

One of the most interesting properties of biochar that makes it attractive as a soil amendment is its porous structure, which is believed responsible for improved water retention and increased soil surface area (Sohi, et al.,2009).

Longer-term benefits for nutrient availability include a greater stabilization of organic matter, concurrent slower nutrient release from the added organic matter and better retention of all cations due to a greater cation exchange capacity (Glaser, 2007). Biochars produced at low temperature have the lowest values of pH and EC

and the highest concentrations of unstable organic carbon and dissolved organic carbon compared with those produced at high temperature (Al-Wabel et al., 2013)

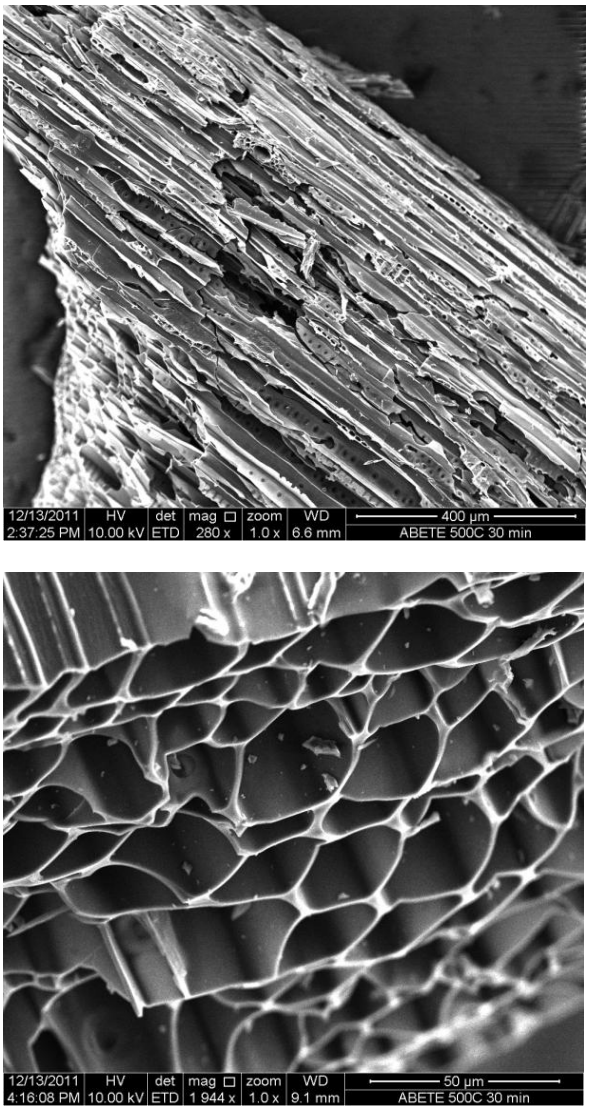

Fig. 5 Biochar from wood sawdust at SEM

Besides the potential of biochar to enhance the fertility of agricultural soils, its apparent ability to increase the capacity of soil to retain water makes biochar a very promising alternative in the current context of climate uncertainty. A high number of

recent studies have highlighted the benefit of using biochar in terms of mitigating global warming and as a strategy to manage soil health and productivity (Manyà, 2012).

In recent study, the field respiration measurements suggested that biochar generally had little effect on SOM mineralization when measured at the whole soil profile level. Similarly, the laboratory incubations also showed little effect of biochar on rates of C turnover (D.L. Jones et al., 2012).

All charcoals, especially high temperature charcoals, were also found to be highly effective at sorbing an organic compound with allelopathic properties

Our results also demonstrate that charcoal is a source of extractable nutrients ($NH4^{+}$, NO^{-3}, and $PO4^{-3}$), bio-available carbon, cation exhchange capacity, and further,may influence the pH and electrical conductivity of forest soils (Gundale, DeLuca, 2007).

To maintain a negative balance in C cycle, obviously, biochar production can not use biomass from deforestation. Slash and burn is a technique used in tropic areas to increase available surface for crop cultivation, but results in a loss of biodiversity and greater amounts of CO_2 being released to the atmosphere from biomass and soil, enhancing the anthropogenic greenhouse effect. (Glaser, 2007).

4.2 Crop productivity

Evaluating the evidence regarding the relationship between biochar and crop productivity, Jefferya et al. (2011) reported an overall relatively small (approximately 10%) but statistically significant, positive effect of biochar

application to soils on crop production. Such a result is robust and useful, as it provides a sound basis for the potential benefits of biochar use on crop productivity.

Agricultural application of biochar would benefit from a characterization framework to identify which biochars produce increases in short and long term yields and improvements in soil health for a given crop and soil (Enders et al.,2012).

The addition of biochar to soil has been associated with an increase of the nutrient use efficiency, either through nutrients contained in biochar or through physicochemical processes that allow better utilization as the increment of cation exchange capacity, altering pH (Xu et al., 2013) of soil-inherent or fertilizer-derived nutrients (Sohi, S.; et al.,2009; Gundale, De Luca, 2006). High content in ashes is a direct contribute to nutrient availability for crops (Glaser, 2007). It was observed that the increasing of soil pH with biochar application may be important for the enhanced P availability (Xu et al., 2013) .

Biochar application to soil enhances soil structure and increases soil porosity, determining a better water retention in fine pores an a consequent reduction of nutrient leaching (Glaser et al., 2002). Gundale and De Luca (2006) demonstrated that charcoal has the capacity to increase net soil N transformations, and that is a extractable nutrients as $NH4^{+}$, $NO3^{-}$, and $PO4^{--}$.

Because of the great variability of biochar properties and of condition of application, Enders et al. (2012) suggested to define first the limiting factors of a particular soil-crop-climate situation and then apply the most suitable biochar on the basis of available literature.

4.2.1 Terra preta

The great interest on biochar end on its application as an amendment to soil started from the study of a part of the territory of Brazil. In fact in several zones along the Rio of Amazones fields characterized by high levels of soil fertility were founded. This territory is known as Amazonian Terra Preta. They are soils are anthropogenic dark earths that were enriched with char >800 years ago; they are more fertile than surrounding soils that received little char input (Mao et al., 2012). 'Terra Preta' soils contained up to 70 times more black carbon than the surrounding soils (Glaser, 2001). These soils, which may occupy up to 10% of Amazonia, are characterized by high levels of soil fertility. The higher fertility of Terra Preta soils results generally in higher crop growth and crop production potential, being about double when compared to adjacent infertile soils (Glaser 2007).

Oxidation during centuries of its polycyclic aromatic structure produced carboxylic groups on the edges of the aromatic backbone, which increased its nutrient-holding capacity. Moreover analysis have shown a higher levels of soil organic matter (SOM), and nutrients such as nitrogen, phosphorus, calcium and potassium, higher pH values and higher moisture-holding capacity than in the surrounding soils (Glaser et al., 2001).

Research on the origin of terra preta revealed that it probably was not intentionally created to improve soil fertility. It is very likely that biochar source did not derive entirely from natural fires or from slush and burn activity, but also from human activity, as cooking, heat production or pottery preparation (Glaser et al., 2012).

4.3. Environmental remediation

An other interesting application of biochar is in environmental remediation. Biochar (BC) produced from agricultural crop residues or dairy manure has proven effective in sorbing organic contaminants as heavy metal Pb and organic contaminant atrazine (Cao et al.,2009). Hydrothermal treatment determines on the biochar surface more oxygen containing groups that have a relevant function in lead sorption (Liu et al., 2009). Biochar capacity to sequester metals is influenced by soil properties, some studies revealed that mechanism of sorption is different in sandy or clay soil, in the latter in fact there is an electrostatic interactions between copper and negatively charged soil and biochar surfaces, sorption on mineral components, complexation of copper by surface functional groups and delocalized π electrons of carbonaceous materials, and precipitation (Uchimiya et al.,2011).

Other results suggest that biochar would have little direct impact on NO_3 leaching, although indirectly the vertical migration of NO_3 might be repressed due to enhanced crop growth and thus greater removal from solution (D.L. Jones et al., 2012).

References:

Cao X., Ma L., Gao B., Harris W. Dairy-Manure Derived Biochar Effectively Sorbs Lead and Atrazine Environ. Sci. Technol. 2009, 43, 3285–3291

Jones D.L., Rousk J.,. Edwards-Jones G,. DeLuca T.H, Murphy D.V. Biochar-mediated changes in soil quality and plant growth in a three year field trial Soil Biology & Biochemistry 45 (2012) 113e124

Enders, A., Hanley, K., Whitman, T., Joseph, S., Lehmann, J., 2012. Characterization of biochars to evaluate recalcitrance and agronomic performance. Bioresour.Technol. 114, 644–653

Glaser B. Prehistorically modified soils of central Amazonia: a model for sustainable agriculture in the twenty-first century Phil. Trans. R. Soc. B (2007) 362, 187–196 doi:10.1098/rstb.2006.1978

Bruno Glaser Ludwig Haumaier Georg Guggenberger Wolfgang Zech The 'Terra Preta' phenomenon: a model for sustainable agriculture in the humid tropics Naturwissenschaften (2001) 88:37–41 DOI 10.1007/s001140000193.

Glaser B., Lehmann J.,·ZechW. Ameliorating physical and chemical properties of highly weathered soils in the tropics with charcoal – a review Biol Fertil Soils (2002) 35:219–230 DOI 10.1007/s00374-002-0466-4

Glaser B., Birk J.J., State of the scientific knowledge on properties and genesis of Anthropogenic Dark Earths in Central Amazonia (terra preta de Indio) Soil Physics Group, University of Bayreuth, 95440 Bayreuth, Germany Geochimica et Cosmochimica Acta 82 (2012) 39–51

Gundale M.J., DeLuca T.H. Temperature and source material influence ecological attributes of ponderosa pine and Douglas-fir charcoal Forest Ecology and Management 231 (2006) 86–

Jefferya S.,. Verheijena F.G.A, van der Veldea M., Bastosc A.C A quantitative review of the effects of biochar application to soils on crop productivity using meta-analysis Agriculture, Ecosystems and Environment 144 (2011) 175–187

Heike Knicker ''Black nitrogen" – an important fraction in determining the recalcitrance of charcoal Organic Geochemistry 41 (2010) 947–950

Liu Z., Zhang F.S. Removal of lead from water using biochars prepared from hydrothermal liquefaction of biomass Journal of Hazardous Materials 167 (2009) 933–939

Manya J.J. Pyrolysis for Biochar Purposes: A Review to Establish Current Knowledge Gaps and Research Needs dx.doi.org/10.1021/es301029g | Environ. Sci. Technol. 2012, 46, 7939−7954

Mao J.-D., Johnson R. L., Lehmann J., Olk D. C., Neves E. G., Thompson M. L., Schmidt-Rohr K. Abundant and Stable Char Residues in Soils: Implications for

Soil Fertility and Carbon Sequestration dx.doi.org/10.1021/es301107c | Environ. Sci. Technol. 2012, 46, 9571−9576

Meyer S., Glaser B., Quicker P. Technical, Economical, and Climate-Related Aspects of Biochar Production Technologies: A Literature Review dx.doi.org/10.1021/es201792c | Environ. Sci. Technol. 2011, 45, 9473–9483

Pratt K., Moran D. Evaluating the cost-effectiveness of global biochar mitigation potential Biomass and Bioenergy 34 (2010) 1149e1158

Preston C. M. Schmidt M. W. I Black (pyrogenic) carbon: a synthesis of current knowledge and uncertainties with special consideration of boreal regions Biogeosciences, 3, 397–420, 2006

Sohi, S.; et al. Biochar, Climate Change and Soil: A Review to Guide Future Research; CSIRO Land and Water Science Report 05/09, 1−56, 2009; http://www.csiro.au/files/files/poei.pdf

Spokas K.A. Review of the stability of biochar in soils: predictability of O:C molar ratios Carbon Management (2010) 1(2), 289–303

Uchimiya M., Klasson K.T., Wartelle L.H., Lima I.M. Influence of soil properties on heavy metal sequestration by biochar amendment:1. Copper sorption isotherms and the release of cations Chemosphere 82 (2011) 1431–1437

Verheijen, F.G.A., Jeffery, S., Bastos, A.C., van der Velde, M., and Diafas, I. (2009). Biochar Application to Soils - A Critical Scientific Review of Effects on Soil Properties, Processes and Functions. EUR 24099 EN, Office for the Official Publications of the European Communities, Luxembourg, 149pp

G. Xu, L.L. Wei, J.N. Sun, H.B. Shao, S.X What is more important for enhancing nutrient bioavailability with biochar application into a sandy soil: Direct or indirect mechanism?. Chang Ecological Engineering 52 (2013) 119–124

5. FAST FIELD CYCLING NMR RELAXOMETRY CHARACTERIZATION OF BIOCHARS OBTAINED FROM AN INDUSTRIAL THERMOCHEMICAL PROCESS

Claudio De Pasquale • Valentina Marsala • Anne E. Berns • Massimo Valagussa • Alessandro Pozzi • Giuseppe Alonzo • Pellegrino Conte

J Soils Sediments (2012) 12:1211–1221 DOI 10.1007/s11368-012-0489-x

5.1 Abstract

Purpose: Biochar has unique properties, which make it a powerful tool to increase soil fertility and to contribute to the decrease of the amount of atmospheric carbon dioxide through the mechanisms of C sequestration in soils. Chemical and physical biochar characteristics depend upon the technique used for its production and the biomass nature. For this reason, biochar characterization is very important in order to address its use either for agricultural or environmental purposes.

Materials and methods: Three different biochars obtained from an industrial gasification process were selected in order to establish their chemical and physical peculiarities for a possible use in agronomical practices. They were obtained by charring residues from the wine-making industry (marc), and from poplar and conifer forests.

Routine analyses such as pH measurements, elemental composition, ash and metal contents were performed together with the evaluation of the CPMAS ^{13}C NMR spectra of all the biochar samples. Finally, relaxometry properties of water

saturated biochars were retrieved in order to obtain information on pore size distribution.

Results and discussion: All the biochars revealed basic pH values due to their large content of alkaline metals. The quality of CPMAS ^{13}C NMR spectra, which showed the typical signal pattern for charred systems, was not affected by the presence of paramagnetic centers. Although paramagnetism was negligible for the acquisition of solid state spectra, it was effective in some of the relaxometry experiments. For this reason no useful information could be retrieved about water dynamics in marc char. Conversely, both relaxograms and nuclear magnetic resonance dispersion profiles of poplar and conifer chars indicated that poplar char is richer in small sized pores, while larger pores appear to be characteristic for the conifer char.

Conclusions: This study showed the potential of relaxometry in revealing chemical-physical information on industrially produced biochar. This knowledge is of paramount importance to properly direct biochar agronomical uses.

Keywords Biochar • CPMAS ^{13}C NMR • FFC NMR • Paramagnetic effect • Relaxometry

5.2 Introduction

"Biochar", "charcoal" and "char" are terms used up to now as synonyms. They all indicate charred organic matter obtained by pyrolysis (or carbonization) of biomasses (Lehmann and Joseph 2009; Brewer et al. 2011; Knicher 2011). However, an attempt to distinguish among them has been recently proposed (Lehmann and Joseph 2009). Namely, both charcoal and biochar are obtained industrially. Nevertheless, while "charcoal" is intended as the material used as fuel for heat, filters, reactant in iron-making and colorant in industry and art, the term "biochar" is referred to all the charred organic systems which are applied deliberately to soils in order to achieve two possible aims: 1. improve fertility, 2. contribute to the mitigation of global climate changes through carbon sequestration into soils (Lehmann and Joseph 2009; Brewer et al. 2011). "Char" is considered as a naturally occurring charred material present in the environment due to vegetation fires (Lehmann and Joseph 2009; Knicher 2011).

From a chemical point of view, all the charred materials are recognized as poly-condensed aromatic systems where the degree of poly-condensation may differ according to the technique used for their production (Warnock et al. 2007; Lehmann and Joseph 2009). As an example, low-temperature-produced charred systems still contain organic compounds that can be used as plant-growth agents. However, low sorption capacity for cations has been observed. Conversely, improvement in sorption capacity with a decrement of plant nutrients has been reported for charred matter retrieved at much higher temperatures (Gundale and DeLuca 2006). In addition, the poly-aromatic macro-molecular structure of charred biomasses is

responsible for their chemical and microbial recalcitrance, which is also the cause for their long mean residence time in soils (Knicker 2011).

The physical characteristics of the charred matter depend on the nature of the biomasses subjected to the thermal stress. In fact, plant species with many large diameter cells in the stem tissues can lead towards biochars containing larger amounts of macropores (Lehmann and Joseph 2009). Macropores in biochar applied to soils may enhance soil draining properties and capacity to retain large molecules such as phenolic compounds (Warnock et al. 2007).

Based on this, we can infer that understanding the chemical and physical properties of biochar is very crucial in order to address its agronomical and environmental uses and allow meaningful pre-application quality assessments.

In the present paper, three biochars obtained from an industrial gasification process were investigated. In particular, they were produced by using conifer and poplar wood chips from forest maintenance, and grape press residues from the wine-making industry. All the biochars were subjected to routine analyses such as pH, elemental and ash content evaluation, and atomic absorption spectroscopy for the measurements of the amount of alkaline metals and paramagnetic Fe, Cu and Mn. Finally, suitability of fast field cycling (FFC) NMR relaxometry was evaluated in order to establish the analytical conditions for the application of this innovative technique in biochar chemistry.

5.3 The industrial thermo-chemical process for biochar achievement

Thermo-chemical conversion of biomasses, also known as gasification, is usually applied to produce stable fuel-gas and charcoal (Dumbleton 1997). During the process, carbonaceous feedstock is partially oxidized by heating at temperatures as high as 1200°C. The gas, generally indicated as syngas, is a mixture of carbon monoxide, carbon dioxide, hydrogen, methane and nitrogen. It is used either to power a diesel-cycle endothermic engine in order to produce both electricity and heat or as a ready-to-use fuel.

The steps occurring during gasification in a temperature gradient can be distinguished in: drying completion, pyrolysis, combustion (i.e. oxidation) and gasification (i.e. reduction).

The first step is simply due to the removal of biomass moisture. Pyrolysis heats up the carbonaceous particles producing volatile compounds and char. After pyrolysis, combustion of volatile compounds and part of the char occurs according to the following reactions:

$O_2 + C \rightarrow CO_2$ $\Delta H = -393\ kJ \cdot mol^{-1}$

$H_2 + O_2 \rightarrow H_2O$ $\Delta H = -242\ kJ \cdot mol^{-1}$

The energy obtained by the aforementioned reactions is used in the last gasification step. It consists in the reduction of the products of combustion (i.e. CO_2, H_2O and some non-combusted partially cracked pyrolysis products) into carbon monoxide, hydrogen and methane through the catalytic action of a red-hot charcoal bed. The reactions involved in the gasification step are as follows:

$C + CO_2 \rightarrow 2\ CO$ $\Delta H = +165\ kJ \cdot mol^{-1}$

$C + H_2O \rightarrow CO + H_2$ $\Delta H = +123\ kJ \cdot mol^{-1}$

$CO + H_2O \rightarrow CO_2 + H_2$ $\Delta H = -42\ kJ \cdot mol^{-1}$

$CO_2 + H_2 \rightarrow CO + H_2O$ $\Delta H = +42\ kJ \cdot mol^{-1}$

$C + 2\ H_2 \rightarrow CH_4$ $\Delta H = -75\ kJ \cdot mol^{-1}$

Gasifiers are classified according to the way air and/or oxygen is introduced (Basu 2010). In the present study, a fixed bed, down draft, open core plant, patented by AGT Advanced Gasification Technology - Italy (PCT/IB2010/054954 Title: Plant and method for the production of gas from biomass), was used to produce charcoal from different feedstock. In the AGT gasifier, air passes through a fixed bed of biomass in the down draft direction and the combustible gases are thrown out in the same way.

The reduction process generates fine-grained, highly porous, pollutant-free charcoal dust, which is collected in a filter (Basu 2010) in order to prevent obstruction of the syngas regular flow in the reactor. Charcoal yield is usually comprised between 5-20% of the parent material (on dry matter base).

5.4 Materials and methods

5.4.1 Biomass samples for biochar production

Biochars were obtained from three different feedstocks: conifer wood chips, poplar wood chips and grape press residues (marc).

Conifer wood chips were the result of mountain forestry management in North Italian Apennines (Valle Staffora, $44°45^{I}15^{II}$ N, $9°13^{I}49^{II}$ E). The tree species

making the biomass feedstock were: Larch (*Larix decidua*), Scots pine (*Pinus sylvestris* L.), Black pine (*Pinus nigra* A.), Silver fir (*Abies alba* M.) and Spruce (*Picea excelsa* L.).

Poplar (*Populus spp.* L.) wood chips were obtained from dedicated short rotation forestry in the Po Valley (Gadesco Pieve Delmona, 45°10^{I}13^{II} N, 10°06^{I}01^{II} E). The age of the forestry at the cutting down was five years.

Grape press residues were the result of a winemaking process in a winery in the centre of Italy (Montefiore dell'Aso, 43°03^{I}57^{II} N, 13°46^{I}52^{II} E). The feedstock included stalks, peels and grape seeds.

5.4.2 Routine chemical characterization

The amounts of carbon and nitrogen were obtained by dry combustion through the use of an elemental analyzer NC 2500 - CE Instrument (Termoquest, Milan, Italy). C and N amounts were corrected for the ash content which was obtained by loss on ignition at a burning temperature of 600°C in an electric muffle furnace (Table 3).

Table 3 Chemical characteristics of the biochars from the industrial thermochemical process

Samples	pH	Ashes	Surface Area
	(in H_2O)	(g Kg^{-1})	(m^2g^{-1})
Marc char	11.1±0.1	360±40	42±4
Poplar char	9.6±0.1	220±20	98±6
Conifer char	10.3±0.1	8.0±0.7	66±5

Samples	C *	N *	Na	K	Ca	Fe	Cu	Mn
	g Kg^{-1}							
Marc char	580±40	16±2	0.2±0.02	9.4±0.4	23.0±0.1	7.5±0.4	0.80±0.04	0.028±0.001
Poplar char	680±50	14±1	0.15±0.01	1.8±0.1	34.0±0.2	0.57±0.03	0.30±00.1	0.035±0.002
Conifer char	760±70	3.9±0.2	0.18±0.02	0.87±0.04	9.8±0.5	1.8±0.1	0.25±0.02	0.032±0.001

*****. Obtained on ash-free basis

Biochar pH was determined in water. Prior to pH measurements, each sample was treated to retrieve the compacted bulk density (CBD) value, which was needed to calculate sample weight to be taken for water suspensions. CBD was determined in a test cylinder with a nominal capacity of 1000 mL and a diameter of 99-105 mm. Here, each fresh sample was subjected to a pressure of 9.17 $g \cdot cm^{-2}$. After suspension in water (specific conductivity ≤ 0.2 $mS \cdot m^{-1}$ at 25°C and a pH $\geq$ 5.6; char-to-water ratio of 1:5, v/v), pH was measured at 22°C with a standard lab pH-meter. pH values are reported in Table 3.

5.4.3 Atomic absorption spectroscopy (AAS)

Milli-Q water (resistivity of 18.2 MΩ·cm at 25°C) used throughout the experiments was produced by a Milli-Q Advantage A10 Ultrapure Water Purification System (Millipore Corporation, Massachusetts, USA). Trace metal grade concentrated nitric and perchloric acids were used together with 30% hydrogen peroxide for digestion of the metals present in the biochar samples. A CEM Mars 5 Microwave Accelerated Reaction System (Bergamo, Italy) was used for digestion by following the procedure described in Tranchina et al. (2008). All reactants were purchased from Sigma (Milan, Italy).

A Shimadzu AA-6300 with flame atomization (Milan, Italy) was used for quantification of total-recoverable levels of paramagnetic (i.e. Cu, Fe and Mn) and alkaline (i.e. Ca, K and Na) metals. The amounts of Cr, Ni, Pb, and Zn were negligible and not further considered in this study. All the measurements were done in triplicates. Table 3 reports the concentrations of Na, K, Ca, Fe, Cu, Mn of the three biochar samples.

5.4.4 CPMAS ^{13}C NMR spectroscopy

Cross polarization magic angle spinning (CPMAS) ^{13}C NMR experiments were carried out on a 7.05 T Varian NMR System (Varian Inc., Palo Alto CA, USA) with a 6 mm Apex HX probe head. The samples were spun at 8500 ± 1 Hz. Between 50000 and 100000 scans were acquired depending on the sample. All free induction decays (FID) were recorded with a recycle delay of 2 s, an acquisition time of 20 ms and a sweep width of 25 kHz. Cross-polarization was performed with a contact time of 5 ms and a ^{13}C r.f. field set at 55 kHz. The ^{1}H r.f. field was centred at the (-1) sideband of the Hartmann-Hahn matching profile at 46.5 kHz and an ascending ^{1}H-ramp of 17 kHz was applied (Berns and Conte 2011). Decoupling was done using a SPINAL sequence with a ^{1}H r.f. field of 54 kHz, a pulse width of 11 µs and a phase of 4.51. The FIDs were acquired with VNMRJ version 2.2D software (Varian Inc., Palo Alto CA, USA) and elaborated with MestReNova 6.1.1 software (Mestrelab Research, Santiago de Compostela, Spain).

5.4.5 NMR Relaxometry

Dried biochars were prepared as slurry for fast field cycling (FFC) NMR relaxometry investigations according to the procedure reported in Dunn et al. (2002). For a detailed description of fast field cycling NMR relaxometry the reader is kindly referred to Kimmich and Anoardo (2004), Anoardo et al. (2001) and Ferrante and Sykora (2005).

^{1}H nuclear magnetic resonance dispersion profiles (i.e. relaxation rates R_1 or $1/T_1$ vs. proton Larmor frequencies) were acquired on a Stelar Smartracer Fast-Field-Cycling Relaxometer (Stelar s.r.l., Mede, PV–Italy) at a constant temperature

of 25°C. The proton spins were polarized at a polarization field (B_{POL}) corresponding to a proton Larmor frequency (ω_L) of 8 MHz for a period of polarization (T_{POL}) corresponding to about five times the T_1 estimated at this frequency. After each B_{POL} application, the magnetic field intensity (indicated as B_{RLX}) was systematically changed in the proton Larmor frequency ω_L comprised in the range 0.01-8.0 MHz. The period τ, during which B_{RLX} was applied, has been varied on 16 logarithmic spaced time sets, each of them adjusted at every relaxation field in order to optimize the sampling of the decay/recovery curves. Free induction decays (FID) were recorded following a single ^{1}H 90° pulse applied at an acquisition field (B_{ACQ}) corresponding to the proton Larmor frequency of 7.20 MHz. A time domain of 100 μs sampled with 512 points was applied. Field-switching time was 3 ms, while spectrometer dead time was 15 μs. For all experiments a recycle delay of 6 s was used. A non-polarized FFC sequence was applied when the relaxation magnetic fields were in the range of the proton Larmor frequencies comprised between 8.0 and 3.0 MHz. A polarized FFC sequence was applied in the proton Larmor frequencies B_{RLX} range of 3.0-0.01 MHz (Kimmich and Anoardo 2004).

5.4.6 FFC NMR data elaboration

R_1 values were achieved by interpolating the ^{1}H magnetization decay/recovery curves at each B_{RLX} value (i.e. ^{1}H signal intensity versus τ) with the stretched exponential function (also known as Kohlrausch-Williams-Watts function) reported in equation [1] after exportation of the experimental data to OriginPro 7.5 SR6 (Version 7.5885, OriginLab Corporation, Northampton, MA, USA). This equation

provided the best fitting with the largest coefficients of determination ($R^2 > 0.998$). The choice of this function was due to the large sample heterogeneity resulting in a multi-exponential behavior of the decay/recovery curves (Morozova-Roche et al. 1999). This approach has the advantage that it is able to handle a wide range of behaviors within a single model. For this reason, assumptions about the number of exponentials to be used in modeling NMRD data are not necessary.

$$I(\tau) = I_0 \exp\left[\left(-\tau/T_1\right)\right]^k \qquad [1].$$

In Eq. [1], I(τ) is the ^{1}H signal intensity at each fixed B_{RLX}, I_0 is the ^{1}H signal intensity at the thermal equilibrium, T_1 is the average proton spin lattice relaxation time and *k* is a heterogeneity parameter related to the stretching of the decay process. This function can be considered as a superposition of exponential contributions, thereby describing the likely physical picture of some distribution in T_1.

Relaxation data at the highest frequency (8 MHz) were also evaluated by UPEN algorithm (Alma Mater Studiorum – Università di Bologna, Italy) (Borgia et al. 1998, 2000) with the aim to obtain the T_1 distributions at this magnetic field and, therefore, information on pore distributions and water interactions. The choice of UPEN analyses only at 8 MHz was due to the larger NMR sensitivity at this frequency as compared to the other proton Larmor frequencies (Kimmich and Anoardo 2004).

The NMRD profiles reporting the calculated R_1 values vs Larmor angular frequency (ω_L) were exported to OriginPro 7.5 SR6 and fitted with a Lorentzian function of the type (Halle et al. 1998; Luchinat and Parigi 2008):

$$R_1 = \alpha + \beta[0.2\frac{\sum_{n=1}^{N} c_n \frac{\tau_n}{1+(\omega_L \tau_n)^2}}{\sum_{n=1}^{N} c_n} + 0.8\frac{\sum_{n=1}^{N} c_n \frac{\tau_n}{1+(2\omega_L \tau_n)^2}}{\sum_{n=1}^{N} c_n}] \qquad [2]$$

In Eq. [2], R_1 is the longitudinal relaxation rate, α represents the high-field relaxation rate and β is a constant related to the dipolar interactions. The latter contains the proton quantum-spin number, the proton gyromagnetic ratio, the Planck constant and the electron-nuclear hyperfine coupling constant which describes the interactions between resonant protons and unpaired electrons. τ is the correlation time, a typical parameter for spectral density which, in turn, describes random molecular motions (Kimmich and Anoardo 2004). Other processes affecting τ are the electronic relaxation times due to the presence of unpaired electrons and the correlation times of surface dynamics and residence of the water protons on the pore surface.

The number *n* of Lorentzians that can be included in equation [2] without unreasonably increasing the number of parameters was determined by means of the merit function analysis (Halle et al. 1998). For the present study, *n*=3 was used for the mathematical fit of the NMRD profiles. The obtained six fit parameters (c_1, c_2, c_3, τ_1, τ_2, τ_3) were used to obtain an average correlation time according to equation [3] (Halle et al. 1998):

$$\langle \tau \rangle = \frac{\sum_n c_n \tau_n}{\sum_n c_n} \qquad [3]$$

Table 4 reports the NMRD parameters obtained by fitting equation [2] and applying equation [3].

Table 4 Values of relaxometry parameters as obtained by applying equations [2] and [3]

Samples	**α (s^{-1})**	**β (x 10^6 s^{-2})**	**$<\tau>$ (x 10^{-6} s^{-1})**
Marc char	5.1±0.5	32±3	0.35±0.03
Poplar char	5.4±0.5	7.6±0.8	1.4±0.1
Conifer char	3.2±0.3	8.1±0.8	0.95±0.08

See the text for the meaning of the relaxometry parameters

5.5 Results and discussion

5.5.1 Biochar inorganic components

Table 3 shows that the pH of the biochar water suspensions is above 9. This can be explained by accounting for the presence of alkaline metals in all the samples (see Table 3). In fact, it is well recognized that sodium (I), potassium (I) and calcium (II) allow an alkaline reaction as the porous media, where they are allocated, are

suspended in a slurry (White 2005). In particular, as biochar is suspended in water, the chemical exchange described in [4] may arise.

$$Biochar-(Na^{+},K^{+},Ca^{2+})_n + nH_2O \rightarrow Biochar-(H^{+})_n + (Na^{+},K^{+},Ca^{2+})_n + nOH^{-} \quad [4]$$

Conversely, iron, copper and manganese cations, also found by AAS in the biochars studied here (see Table 3), are involved in the acid reaction reported in the chemical equation [5] where Me^{n+} can be one of the three transition metals in any of their oxidation states.

$$Me^{n+} + nH_2O \rightarrow Me(OH)_n + nH^{+} \quad [5]$$

The predominance of the basic over the acid reaction as supported by the pH values in Table 3 is a clear indication that Na^{+}, K^{+} and Ca^{2+} are exchanged with the water protons, thereby suggesting that the aforementioned alkaline cations are mainly adsorbed on the biochar surface. Conversely, iron, copper and manganese are conceivably present as oxides in the biochar ashes thus making the contribution of [5] to the biochar reaction in water negligible.

5.5.2 Biochar CPMAS ^{13}C NMR structural features

Paramagnetic metals (such as for example Fe (III), Cu (II) and Mn (VII)) affect the reliability of NMR spectra by increasing the rate of the relaxation mechanisms to such an extent that NMR signals lower and broaden, thereby disappearing. Although paramagnetic ions have only short range effects since paramagnetism only operates within the distance of a few bonds from the paramagnetic centers, unacceptable CPMAS ^{13}C NMR spectra can be recorded when

the Fe/C ratio (w/w) is »1 (Preston 1996; Smernik and Oades 2000 a, b; Conte et al. 2001, 2004).

The amount of paramagnetic metals (Fe, Cu and Mn) revealed in the inorganic part of the biochars studied here, is from 2 to 3 orders lower than the amount of carbon content (see Table 3). For this reason, the Fe/C, Cu/C and Mn/C ratios are «1 for all the samples. Because of this, we can neglect paramagnetism effects in CPMAS ^{13}C NMR spectra acquisition and reasonably assume that the spectra reported in Fig. 6 are representative of the chemical composition of each sample.

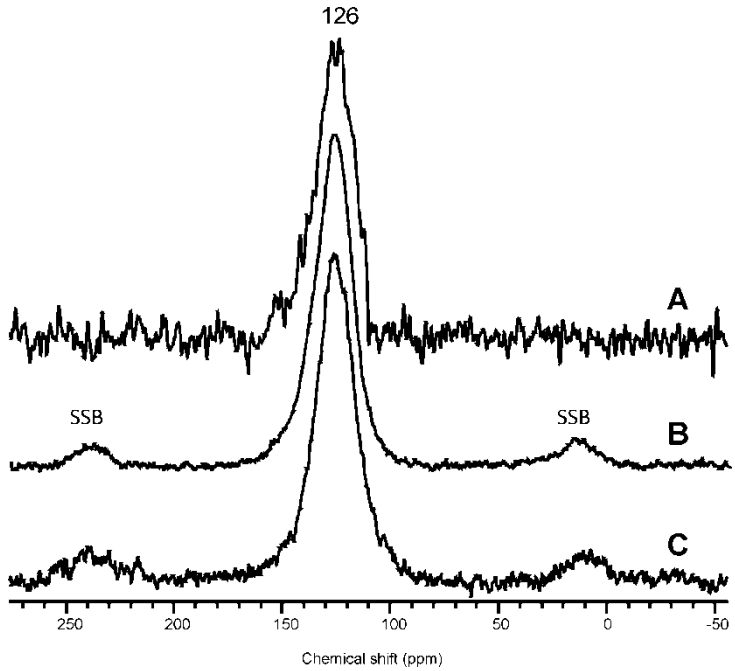

Fig. 6 CPMAS 13C NMR spectra of A. marc char, B. poplar char and C. conifer char. SSB are the spinning side bands.

As a general remark, it is well known that the aromatic condensation in chars increases as the heat treatment temperature rises up (McBeath and Smernik 2009).

Our results confirm these literature findings because only one broad band at 126 ppm was observed in the CPMAS ^{13}C NMR spectra of marc, poplar and conifer chars (see Fig. 6). According to Krull et al. (2009), McBeat and Smernik (2009) and Knicker (2011), the signal at 126 ppm is due to the diamagnetic currents produced by delocalized π-electrons in extended aromatic structures or graphite-like micro-crystallites. For this reason conversion of biomasses to biochar (i.e. graphite-like structure) at the temperature of around 1200°C reached in the gasifier described above can be considered complete.

5.5.3 ^{1}H T_1 relaxograms

Distributions of longitudinal relaxation times (T_1) at a fixed proton Larmor frequency (i.e. 8 MHz in the present study) are traditionally related to the porosity of porous media (Pohlmeier et al. 2009).

T_1 is the lifetime of the first order rate process that returns the ^{1}H magnetization to the Boltzman equilibrium (Bakhmutov 2004). Its magnitude depends on the nature of the nuclei, the physical state of the system and the temperature. In particular, spin–lattice (or longitudinal) relaxation occurs when the lattice experiences magnetic fields fluctuating at frequencies resembling those of the observed nuclei (e.g. protons). Fluctuating fields are generated by molecular motions that strongly affect dipolar interactions. Namely, in the fast motion regime ($1 \gg \omega_0^2 \tau_C^2$), which is the case of the low field NMR applied here, the faster the motions are (e.g., water in large sized pores), the lower is the dipolar interaction efficiency, thereby favoring longer T_1 values. Conversely, slower molecular dynamics (as for water constrained in small sized pores) can be associated with

shorter spin–lattice relaxation times due stronger nuclear dipolar interactions (Bakhtumov 2004; Pohlmeier et al. 2009).

Biochar structure and porosity is strongly dependent upon that of the parent material. In fact, according to the proportions of hemicelluloses, celluloses and lignin in biomasses, the thermal processes occurring during charring produce biochars with different physical properties (Downie et al. 2009). Moreover, also amount and nature of the inorganic components (i.e. ashes) have implications for the physical biochar structures. As an example, some processing conditions result in ash fusion or sintering that can induce dramatic changes within the physical and structural biochar composition (Downie et al. 2009).

Fig. 7 reports the relaxograms for marc (MC), poplar (PC) and conifer (CC) chars. The relaxograms are broad and entangled, spanning several T_1 decades with the amplitudes (A) changing in the order $A_{MC}>A_{PC}>A_{CC}$ (see Fig. 7). This is also the trend for the ash contents: $ash_{MC}>ash_{PC}>ash_{CC}$ (see Table 3). Conversely, carbon and nitrogen change in the order $C_{CC}>C_{PC}>C_{MC}$ and $N_{MC}\sim N_{PC}>N_{CC}$ (Table 3).

Based only on the relaxation mechanism stated above, we may suggest that the widest amplitude of the marc char relaxogram indicates that the MC pore distribution is wider than in the other two samples. In particular, two maxima can be identified in Fig. 7A. The first one at the shortest T_1 value (78 ms) can be due to water molecules diffusing in the smallest sized pores, whereas the water trapped in the largest sized pores generates the T_1 maximum at 664 ms (see Fig. 7A).

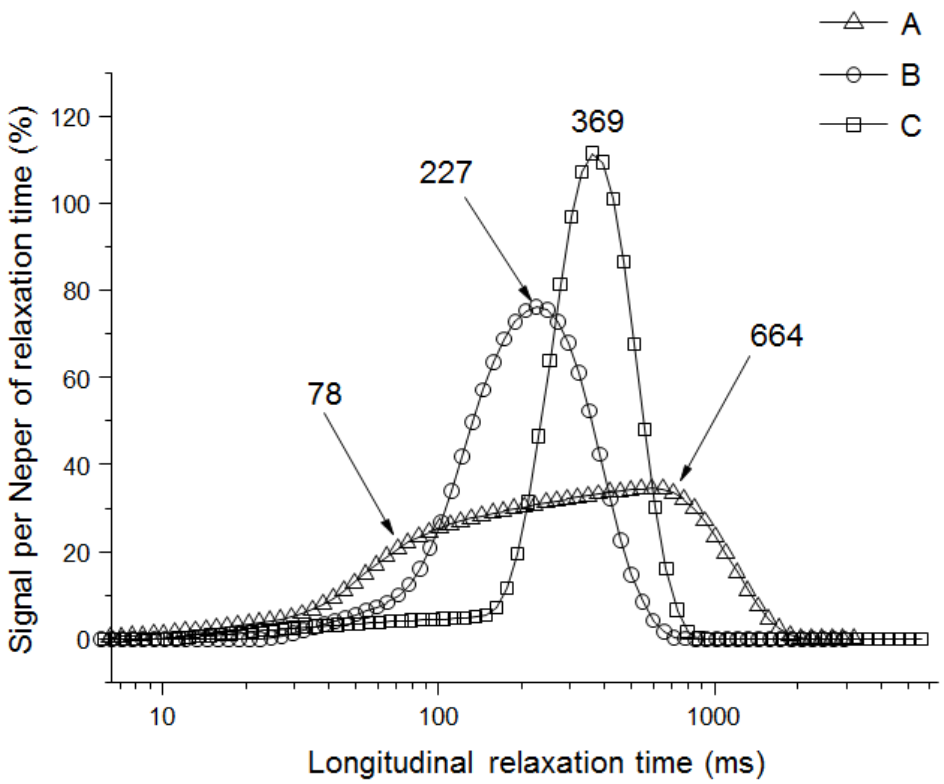

Figura 7 Spin-lattice relaxation time (T1) distributions of the water saturated A. marc char, B. poplar char and C. conifer char obtained at the proton Larmor frequency of 8 MHz

On the other hand, both PC and CC samples revealed symmetric T_1 distributions with the maximum in PC relaxogram centered at 227 ms (see Fig. 7B), and that in CC relaxogram at 369 ms (see Fig. 7C). Symmetry of PC and CC relaxograms can be attributed to larger pore size homogeneity as compared to the MC sample. However, according to the ash findings reported in Table 3, we can suggest that the T_1 distributions in Fig. 7 are dependent more on the amounts of inorganic components than on those of the organic carbon and nitrogen. Noteworthy, the amount of paramagnetic centers (i.e. Fe, Cu and Mn) in the ashes is larger in MC than in PC and CC (Table 3). For this reason, in contrast with the

traditional aforementioned relaxogram interpretation, we can advise that the MC T_1 distribution (see Fig. 7A) does not represent a pore size distribution as for PC (Fig. 7B) and CC (Fig. 7C) relaxograms. In fact, the relaxation rates of liquids in proton-poor solids (such as biochars) are dependent on the translational diffusion of the liquid in the neighborhood of the solid surfaces (Korb 2011). Since these surfaces can be rich in paramagnetic centers (such as in the case of marc char), the magnetic moments and the local dipolar fields generated by the un-paired electrons accelerate relaxation rates of the proton spins in the diffusing water. For this reason, alteration of the meaning of the T_1 distributions arises. In the case of Fig. 7A, the short T_1 values cannot be due only to water trapped in small sized pores, but also to the effect of paramagnetic centers conceivably present in the MC ashes. On the other hand, due to the lower amounts of paramagnetic centers, the different positions of PC and CC relaxograms (Fig. 7B and 7C, respectively) can be attributed to a dissimilar pore size distribution. Namely, poplar char is richer in small sized pores, whereas large pore sizes appear to be characteristic for the conifer char.

5.5.4 Qualitative and quantitative aspects of NMRD profiles

Fig. 8 reports the NMRD profiles of marc, poplar and conifer chars. It shows that the longitudinal relaxation rates vary in the order: $R_{1(MC)}>R_{1(PC)}>R_{1(CC)}$ in the whole range of the proton Larmor frequencies (0.01-8 MHz) investigated in the present study.

According to the discussion above, the fastest $R_{1(MC)}$ is due to the larger amount of paramagnetic metals in marc char ashes as compared to those found in poplar and conifer chars (Table 3)

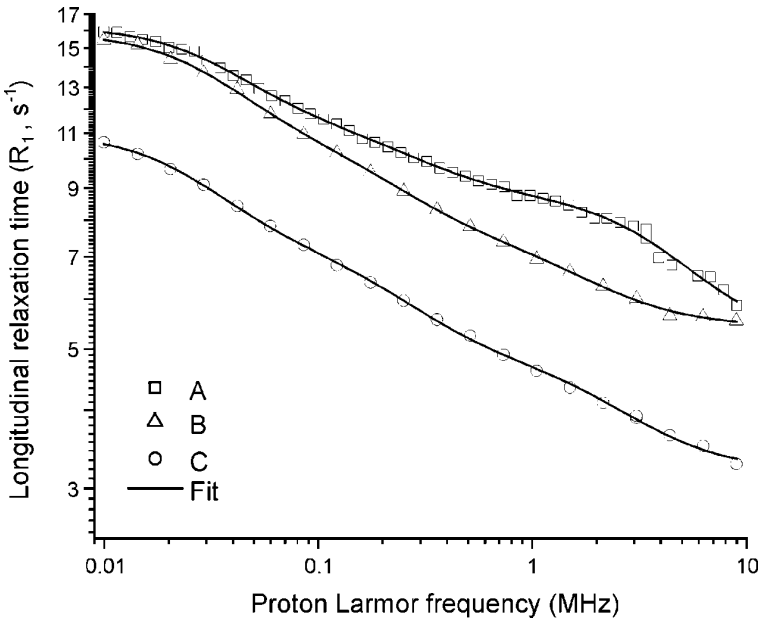

Fig. 8 NMRD profiles of A. marc char, B. poplar char and C. conifer char

. On the other hand, the different longitudinal relaxation rates measured for the water saturated PC and CC systems can be explained by considering water mobility in different sized pores. In fact, as stated above, pore sizes in poplar char are, in average, smaller than in conifer char. For this reason, the more constrained PC water undergoes faster relaxation rates than the freely moving water in CC suspension.

The qualitative evaluation of the NMRD profiles in Fig. 8 is also confirmed by their quantitative assessment through application of equations [2] and [3].

Table 4 reports the values of three relaxometry parameters (α, β and $<\tau>$) for the water saturated chars investigated here.

α is the relaxation rate at the high field plateau of the NMRD profiles (Kimmich and Anoardo 2004). The shorter the α value, the less constrained are the

water molecules into porous media due to weak dipolar interactions. On the other hand, when water is tightly bound to biochars, dipolar interactions become stronger and relaxation rates become faster (Bakhtumov 2004).

β is a measure of the force of the ^{1}H-^{1}H dipolar interactions (Halle et al. 1998; Luchinat and Parigi 2008). Increasing dipolar strengths, due to reduced water mobility, produce larger β values. Conversely, weak dipolar couplings are generated by unbound (or freely moving) water, thereby providing smaller β values.

The average correlation time $<\tau>$ as obtained by equation [3] is associated to the rate of molecular reorientation in the time unit (Bakhtumov 2004). Namely, slower molecular motions, due to bound water molecules, produce larger $<\tau>$ values, whereas shorter $<\tau>$ values are related to fast molecular movements.

Due to the larger amount of paramagnetic centers, the MC values of the three relaxometry parameters reported in Table 4 cannot be compared to those retrieved for the water diffusing in poplar and conifer chars. In fact, as protons interact with paramagnetic centers, the contribution of the electron Larmor frequency, the electron g-factor and the Bohr magneton in α and β cannot be neglected (Bakhtumov 2004). In addition, the correlation times of diffusing water in paramagnetic media are affected by the contribution of the electron spin relaxation times (Bakhtumov 2004). For this reason, a comparison between α, β and $<\tau>$ values of water saturated marc, and those retrieved for the water diffusing in poplar and conifer chars is not possible. Conversely, PC and CC relaxometry parameters can be compared to each other. In particular, Table 4 shows that $\alpha_{PC}>\alpha_{CC}$ and $<\tau>_{PC} > <\tau>_{CC}$. These findings are as expected considering PC pores smaller than CC ones.

Due to the large fitting errors (see Table 4), the β values of both water saturated PC and CC systems resulted similar to each other, thereby preventing any possible differentiation among them.

5.6 Conclusions

The present paper reports a chemical and spectroscopic characterization of three chars obtained as by-products of an industrial gasification process. All the chars revealed a basic pH reaction due to their large ash content rich in alkaline metals (see Table 3). This result, which is in line with other literature data for high-temperature-achieved chars (e.g. Lima et al. 2009), suggested that the alkaline metals are mainly adsorbed on char surfaces. On the other hand, the negligible effect of other Lewis acids, such as the paramagnetic Fe, Cu and Mn, on the pH values of the water saturated chars indicates that the latter are probably present in the form of stable oxides.

The atomic absorption spectroscopy results were used to roughly estimate the paramagnetic-to-carbon (P-to-C) ratios in order to verify the reliability of the biochar CPMAS ^{13}C NMR spectra. Since P-to-C ratios resulted «1 for all the samples, we assumed that the ^{13}C solid state high field NMR spectra were representative of the chemical composition of the samples under investigation (see Fig. 5). According to Krull et al. (2009), McBeat and Smernik (2009) and Knicker (2011) the complete high temperature charring of conifer wood chips, poplar wood chips and grape press residues (i.e. marc) produced polycondensed aromatic structures responsible for the sole signal at 126 ppm. Notwithstanding the different nature of the biomasses used for biochar production, the CPMAS ^{13}C NMR

spectroscopy was unable to reveal substantial structural dissimilarities among chars. Conversely, application of fast field cycling NMR relaxometry on water saturated chars revealed differences that were explained either by accounting for the amount of inorganic paramagnetic centres or for the different pore size distributions. Namely, the char obtained from marc revealed the largest content of ashes and potentially paramagnetic centres (see Table 3). For this reason, its ^{1}H T_1 relaxogram showed the widest T_1 width (see Fig. 7) and the MC relaxometry parameters were incomparable with those from PC and CC (see Table 4). Conversely, due to the lower amounts of ashes and paramagnetic centres (see Table 3), the relaxograms of the latter two samples (see Fig. 7) differed because of their pore size distributions. In fact, both qualitative and quantitative evaluation of fast field cycling NMR results supported the conclusion that poplar char was made by a larger number of small sized pores as compared to the char retrieved from conifer residues.

From an analytical point of view, this study evidenced that care must be used when interpreting relaxometry data from charred biomasses. In fact, even if the paramagnetic content of each sample studied here was insufficient to efficaciously affect acquisition of high resolution solid state ^{13}C NMR spectra, FFC NMR relaxometry was strongly influenced by both ash content amount and nature. For this reason, a careful evaluation of the chemical composition of biochars must be carried out prior to any possible relaxometry data interpretation. Finally, it must be stated that this is a preliminary study revealing the suitability of FFC NMR relaxometry in providing information on the physical properties of three industrial biochars obtained from a gasification process applied for energy production. It represents the

base for the understanding of the potential uses of such industrial by-products in environmental applications (Brewer et al. 2011).

Acknowledgments P. C. acknowledges Forschungszentrum Jülich GmbH (Germany) for having invited him as visiting scientist at the NMR centre of the Institute of Bio- and Geosciences, IBG-3: Agrosphere. FFC NMR measurements were done at the Università degli Studi di Palermo.

References

Anoardo E, Galli, G, Ferrante G (2001) Fast-Field-Cycling NMR: Applications and Instrumentation. Applied Magn Reson 20:365-404

Bakhmutov VI (2004) Practical NMR relaxation for chemists. Wiley, Chichester

Basu P (2010) Biomass Gasification and Pyrolysis: Practical Design and Theory. Academic Press, ISBN: 9780123749888

Berns AE, Bubici S, De Pasquale C, Alonzo G, Conte P (2011) Applicability of solid state fast field cycling NMR relaxometry in understanding relaxation properties of leaves and leaf-litters. Org Geochem doi:10.1016/j.orggeochem.2011.04.006

Berns AE, Conte P (2011) Effect of ramp size and sample spinning speed on CPMAS ^{13}C NMR spectra of soil organic matter. Org Geochem doi:10.1016/j.orggeochem.2011.03.022

Borgia GC, Brown RJS, Fantazzini P (1998) Uniform-Penalty Inversion of Multiexponential Decay Data. J Magn Reson 132:65-77

Borgia GC, Brown RJS, Fantazzini P (2000) Uniform-Penalty Inversion of Multiexponential Decay Data: II. Data Spacing, T2 Data, Systematic Data Errors, and Diagnostics. J Magn Reson 147:273-285

Brewer CE, Unger R, Schidt-Rohr K, Brown RC (2011) Criteria to select biochars for field studies based on biochar chemical properties. Bioenerg Resour doi:10.1007/s12155-011-9133-7

Conte P, Piccolo A, van Lagen B, Buurman P, Hemminga MA (2001) Effect of residual ashes on CPMAS-^{13}C NMR spectra of humic substances from volcanic soils. Fresenius Environ Bull 10:368-374

Conte P, Spaccini R, Piccolo A (2004) State of the art of CPMAS ^{13}C-NMR spectroscopy applied to natural organic matter. Prog Nucl Magn Reson Spectrosc 44:215–223

Conte P, Maccotta A, De Pasquale C, Bubici S, Alonzo G (2009) Dissolution Mechanism of Crystalline Cellulose in H_3PO_4 As Assessed by High-Field NMR Spectroscopy and Fast Field Cycling NMR Relaxometry. J Agr Food Chem 57:8748–8752.

Downie A, Crosky A, Munroe P (2009) Physical properties of biochar. In: Lehmann J, Joseph S (eds) Biochar for environmental management: science and technology, Earthscan publisher, London UK, pp 13-33

Dumbleton F (1997) Biomass conversion technologies: An overwiew. Aspect Appl Biol 49:341-347

Dunn KJ, Bergman DJ, Latorraca GA (2002) Handbook of geographic exploration-seismic exploration: nuclear magnetic resonance petrophysical and logging applications. Elsevier Science Ltd, Oxford, UK

Ferrante G, Sykora S (2005) Technical aspects of fast field cycling. Adv Inorg Chem 57:405-470

Gundale MJ, De Luca TH (2006) Temperature and source material influence ecological attributes of ponderosa pine and Douglas-fir charcoal. For Ecol Manage 231:86-93

Halle B, Johannesson H, Venu K (1998) Model-Free Analysis of stretched relaxation dispersions. J Magn Reson 135:1-13.

Kiihne S, Bryant RG (2000) Protein-Bound Water Molecule Counting by Resolution of ^{1}H Spin-Lattice Relaxation Mechanism. Biophysical J 78:2163-2169.

Kimmich R, Anoardo E (2004) Field-cycling NMR relaxometry. Prog Nucl Magn Reson Spectrosc 44: 257–320

Knicher H (2011) Pyrogenic organic matter in soil: its origin and occurrence, its chemistry and survival in soil environments. Quater Int doi:10.1016/j.quaint.2011.02.037

Korb JP (2011) Nuclear magnetic relaxation of liquids in porous media. New J Phys 13:035016

Krull ES, Baldock JA, Smernik RJ, Skjemstad O (2009) Characteristics of Biochar: Organo-chemical Properties. In: Lehmann J, Joseph S (eds.) Biochar for environmental management: science and technology, Earthscan publisher, London UK pp 53-63

Lehmann J, Joseph S (2009) Biochar for environmental management: an introduction. In: Lehmann J, Joseph S (eds.) Biochar for environmental management: science and technology, Earthscan publisher, London UK pp 1-13

Lima IM, Boateng AA, Klasson KT (2009) Pyrolisis of broiler manure: char and product gas characterization. Ind Eng Chem Res 48:1292-1297

Luchinat C, Parigi G (2008) Nuclear Relaxometry Helps Designing Systems for Solution DNP on Proteins. Appl Magn Reson 34:379-392

McBeath AV, Smernik RJ (2009) Variation in the degree of aromatic condensation of chars. Org Geochem 40:1161-1168

Morozova-Roche LA, Jones JA, Noppe W, Dobson CM (1999) Independent Nucleation and Heterogeneous Assembly of Structure during Folding of Equine Lysozyme. J Mol Biol 289:1055-1073.

Pohlmeier A, Haber-Pohlmeier S, Stapf S (2009) A Fast Field Cycling Nuclear Magnetic Resonance Relaxometry Study of Natural Soils. Vadose Zone J 8:735-742

Preston CM (1996) Applications of NMR to soil organic matter analysis: history and prospects. Soil Sci 161:144-166

Smernik RJ, Oades JM (2000a) The use of spin counting for determining quantitation in solid state [sup.13]C NMR spectra of natural organic matter. 1. Model systems and the effects of paramagnetic impurities. Geoderma 96:101-129

Smernik RJ, Oades JM (2000b) The use of spin counting for determining quantitation in solid state [sup.13]C NMR spectra of natural organic matter. 2. HF-treated soil fractions. Geoderma 96:159-171

Tranchina L, Basile S, Brai M, Caruso A, Cosentino C, Miccichè S (2008) Distribution of Heavy Metals in Marine Sediments of Palermo Gulf (Sicily, Italy). Water Air Soil Pollut 191:245–256

Warnock DD, Lehmann J, Kuyper TW, Rilling MC (2007) Mycorrhizal responses to biochar in soil – concepts and mechanisms. Plant Soil 300:9-20

White RE (2005) Principles and practice of soil science: the soil as a natural resource. Blackwell Publishing, Malden MA, USA 4th edition

6. NATURE OF WATER-BIOCHAR INTERFACE INTERACTIONS

Pellegrino Conte, Valentina Marsala, Claudio De Pasquale, Salvatore Bubici, Massimo Valagussa , Alessandro Pozzi and Giuseppe Alonzo

GCB Bioenergy (2012), doi: 10.1111/gcbb.12009

6.1 Abstract

A poplar biochar obtained by an industrial gasification process was saturated with water and analyzed using fast field cycling (FFC) NMR relaxometry in a temperature range between 299 and 353 K. Results revealed that the longitudinal relaxation rate increased with the increment of the temperature. This behavior was consistent with that already observed for paramagnetic inorganic porous media for which two different relaxation mechanisms can be accounted for: outer- and inner-sphere mechanisms. The former is due to water diffusing from the closest approach distance to infinity, whereas the second is due to water interacting by nonconventional H-bonds to the porous surface of the solid material. In particular, the inner-sphere relaxation appeared to be predominant in the water-saturated biochar used in the present study. This study represents a fundamental first step for the full comprehension of the role played by biochar in the draining properties of biochar-amended soils.

Keywords: biochar, char, fast field cycling NMR, gasification, longitudinal relaxation time, NMRD, relaxometry

6.2 Introduction

Biochar (BC) is a charred organic material, which is applied deliberately to soils to improve fertility and to contribute to the mitigation of global climate changes through carbon sequestration in soils (Lehmann &

Joseph, 2009; Brewer et al., 2011; De Pasquale et al., 2012). From a chemical point of view, BC is recognized as a poly-condensed aromatic system where the degree of poly-condensation may differ according to the technique used for its production (Warnock et al., 2007; Lehmann & Joseph, 2009).

Clarkson et al. (1998) depicted biochar as a porous material rich in paramagnetic centers having both inorganic and organic nature. In particular, the inorganic paramagnetic centers originate from the metals (e.g. Fe, Cu, Mn etc.) usually present in the biomasses used for biochar production. Conversely, the organic paramagnetism is due to the unpaired electrons of the delocalized π-system generated during the charring reactions (De Pasquale et al., 2012). Paramagnetic centers are distributed among surface-sites, also referred to as α-type, and bulk-sites, also indicated as β–types (Clarkson et al., 1998). As biochar is water-saturated, water can flow between the α and β type sites through diffusional processes, which can be hampered physically by the pore sizes and chemically by the solid-liquid interactions (Clarkson et al., 1998; Belford et al., 2000). The latter, in turn, are described as hydrogen bonds between the oxygen of water and the hydrogen atoms of the biochar aromatic systems (Clarkson et al., 1998). However, Belford et al. (2000) also indicated that possible water-biochar interactions can occur between the electron-deficient orbitals of the hydrogen atoms in water and the orbitals containing

the unpaired electrons of both the inorganic and organic paramagnetic centers. These interactions were also hypothesized by other authors who examined the surface properties of paramagnetic silica-based porous materials (Korb, 2001, 2006). Apart from the diffusion between the α and β type sites, water can also escape by the biochar surface toward the bulk solution. Nuclear magnetic resonance (NMR) techniques are applied to recognize the dynamic properties of complex systems (Conte et al., 2004; Kimmich & Anoardo, 2004). In particular, longitudinal or spin-lattice relaxation rates (R1) are the physical NMR parameters measured to retrieve information on molecular dynamics. In fact, spin-lattice relaxation occurs when the lattice experiences magnetic fields fluctuating at frequencies resembling those of the observed nuclei (e.g. protons) Fluctuating fields are generated by molecular motions, which strongly affect dipolar interactions (Bakhmutov,2004). However, it must be stated that single measurements are not sufficient to assess a complete understanding of the dynamical properties of a complex molecular system at a fixed magnetic field strength, such as in the high field (or high resolution) NMR spectroscopy. In fact, relaxation rates are related to both spectral densities [J(ω)] at the appropriate magnetic field frequency and the strength (C) of the dipolar interactions being modulated. Both J(ω) and C can be fully evaluated only by running relaxometry experiments at different temperatures, due to the strict dependence of R1 values upon temperature (T) variations (Bakhmutov, 2004). Nevertheless, this approach can be routinely applied only when temperature alterations of the matrices under investigation are not attainable. Alternatively, molecular dynamics can be monitored through the modulation of the applied magnetic fields such as in fast field cycling (FFC) NMR relaxometry (Kimmich & Anoardo, 2004). The latter technique is

considered as a powerful tool for monitoring water dynamics in porous systems with a wide variety of different chemical-physical properties (Korb, 2001, 2006; Kimmich & Anoardo, 2004; De Pasquale et al., 2012; Laudicina et al., 2012). In our previous article (De Pasquale et al., 2012) we have already suggested that relaxometry applied on water-biochar systems allow to distinguish BC pore size distributions. However, we also stated that paramagnetism prevents achievement of an absolute value for BC pore sizes. In the present study, we intend to show that paramagnetism can be used to monitor the nature of the interactions at the water-biochar interface. This goal is a very important step for the full comprehension of the role played by biochar in the water dynamics in BC-amended soils. We will make use of the knowledge about FFC NMR properties of paramagnetic inorganic materials for which very suitable physical models have been already produced (Korb, 2001, 2006; Alhaique et al., 2002; Strijkers et al., 2005; Caravan, 2006; Caravan et al., 2007; Gossuin et al., 2008; Laurent et al., 2008).

6.3 Materials and methods

The biochar sample was obtained from poplar (Populus spp. L.) wood chips, which were in turn, retrieved from dedicated short rotation forestry in the Po Valley (Gadesco Pieve Delmona, 45 ° 10′13″ N, 10 °06′01″ E). The age of the forestry at the cutting down was 5 years. The gasification process applied for biochar production and the routine analyses for poplar biochar characterization have been already reported in De Pasquale et al.(2012).

Fast field cycling NMR experiments

The dried poplar biochar has been prepared as slurry for FFC NMR relaxometry investigations according to the procedure reported in Dunn et al. (2002). The theory describing FFC NMR relaxometry can be found in Anoardo et al. (2001), Kimmich & Anoardo (2004), Ferrante & Sykora (2005). The theory about the pulse sequence applied in the present study has been described in De Pasquale et al. (2012). 1H nuclear magnetic resonance dispersion profiles (i.e. relaxation rates R1 or 1/T1 vs. proton Larmor frequencies) were acquired on a Stelar Spinmaster FFC2000 Relaxometer (Stelar s.r.l.; Mede, PV, Italy) at temperatures of 299, 309, 323, 333, 343, and 353 K. The proton spins were polarized at a polarization field (BPOL) corresponding to a proton Larmor frequency (L) of 24 MHz for a period of polarization (TPOL) corresponding to about five times the T1 estimated at this frequency. After each BPOL application, the magnetic field intensity (indicated as BRLX) was systematically changed in the proton Larmor frequency L comprised in the range 0.01–39.0 MHz. The period τ, during which BRLX was applied, has been varied on 32 logarithmic spaced time sets, each of them adjusted at every relaxation field to optimize the sampling of the decay/recovery curves. Free induction decays (FID) were recorded following a single 1 H90° pulse applied at an acquisition field (BACQ) corresponding to the proton Larmor frequency of 16 MHz. A time domain of 100 s sampled with 512 points was applied. Field-switching time was 3 ms, whereas spectrometer dead time was 15 s. For all experiments a recycle delay of 12 s was used. A non-polarized FFC sequence was applied when the relaxation magnetic fields were in the range of the proton Larmor frequencies comprised between 39.0 and 9.0 MHz. A polarized FFC sequence was applied in the proton Larmor frequencies BRLX range of 9.0–0.01 MHz (Kimmich & Anoardo, 2004).

FFC NMR data elaboration

R1 values were achieved by interpolating the ^{1}H magnetization decay/recovery curves at each BRLX value (i.e. 1H signal intensity vs. τ) with the stretched exponential function (also known as Kohlrausch–Williams–Watts function) reported in Eqn (6) after exportation of the experimental data to OriginPro 7.5 SR6 (Version 7.5885; OriginLab Corporation, Northampton, MA, USA). This equation provided the best fitting with the largest coefficients of determination (R2> 0.998). The choice of this function was due to the large sample heterogeneity resulting in a multi-exponential behavior of the decay/recovery curves (Morozova-Roche et al., 1999). This approach has the advantage that it is able to handle a wide range of behaviors within a single model. For this reason, assumptions about the number of exponentials to be used in modeling NMRD data are not necessary.

$$I(\tau) = I_0 \exp\left[-(\tau/T_1)^k\right] \qquad [6].$$

In Eqn (6), I(τ) is the 1 H signal intensity at each fixed BRLX, I0 is the 1

H signal intensity at the thermal equilibrium, T1 is the average proton spin-lattice relaxation time, and k is heterogeneity parameter related to the stretching of the decay process. This function can be considered as a superposition of exponential contributions, thereby describing the likely physical picture of some distribution in T1. The NMRD profiles reporting the calculated R1 values vs. Larmor angular

frequency (L) were exported to OriginPro 7.5 SR6 and fitted with a Lorentzian function of the type (Halle et al., 1998):

$$R_1 = \frac{\sum_{n=1}^{N} c_n \frac{\tau_n}{1+(\omega_L \tau_n)^2}}{\sum_{n=1}^{N} c_n} \quad [7]$$

In Eqn (7), R1 is the longitudinal relaxation rate, τ is the correlation time, a typical parameter for spectral density which, in turn, describes random molecular motions (Kimmich & Anoardo, 2004; De Pasquale et al., 2012). The number n of Lorentzians that can be included in Eqn (7) without unreasonably increasing the number of parameters was determined by means of the Merit function analysis (Halle et al., 1998). For the present study, n = 4 was used for the mathematical fit of the NMRD profiles. This contrasts with the description of the NMRD profiles in De Pasquale et al. (2012) where a three-component Eqn (7) was applied. The difference between the present study and that reported in De Pasquale et al. (2012) consists in the spanned magnetic field range. In fact, in the previous article the magnetic field interval 0.01–10 MHz was investigated. In this study, the magnetic field range was expanded up to 39 MHz. This was possible due to the use of two different NMR instruments. In De Pasquale et al. (2012) we used a Stelar Smartracer FFC NMR relaxometer, which allows to investigate only up to a magnetic field of 10 MHz. Here we used a more powerful Stelar Spinmaster FFC2000 relaxometer (see above) that can span magnetic fields up to 40 MHz. For this reason, the application of the

three-component Eqn (7) used in De Pasquale et al. (2012) proved unsuccessful here. The obtained eight fit parameters (c1,c2,c3,c4, τ1, τ2, τ3, τ4) were used to retrieve an average correlation time according to Eqn (8) (Halle et al., 1998):

$$\langle \tau_C \rangle = \frac{\sum_n c_n \tau_n}{\sum_n c_n} \qquad [8]$$

6.4 Results

Nuclear magnetic resonance relaxometry experiments were conducted at variable temperature and at different magnetic field strengths by applying a fast field cycling NMR setup (see above in Materials and methods). The experiments performed at the proton Larmor frequency of 39 MHz revealed that the proton longitudinal relaxation time values of water in the water-biochar system were directly proportional to the inverse of the temperature (Fig. 9). This feature was further confirmed in the whole 1H Larmor frequency range chosen for the FFC NMR experiments as reported in Fig. 10. In fact, the NMRD profiles (Fig. 10) revealed that increment of the longitudinal relaxation rates (R1 = 1/T1, as stated in Materials and methods) was obtained as temperature was changed from 299 to 353 K. The advantage in carrying variable temperature experiments at different proton Larmor frequencies lays the possibility to retrieve Arrhenius graphs such as those reported in Figs 11 and 12. The latter, in particular, was obtained by monitoring the temperature dependence of the correlation times calculated according to Eqn (8). Arrhenius graphs allow achievement of the activation energy (see Discussion below)

for the physical-chemical processes (described either by the R1 values in Fig. 11 or by the <τC> values in Fig. 12) occurring in the water-biochar system as temperature is varied (see Discussion below).

6.5 Discussion

As water saturates a porous material, two different proton longitudinal relaxation mechanisms can be recognized. The first one is indicated as outer-sphere relaxation mechanism. It is described by the outer-sphere longitudinal relaxation rate (R1out = 1/T1out). This relaxation mechanism is due to the water diffusing by the biochar surface, from a distance d, indicated as distance of closest approach (Hwang & Freed, 1975), and infinity. This diffusion occurs when weakly bound water is replaced by other similar molecules belonging to the bulk water system. From a mathematical point of view, R1out is related to the diffusion constant (D), the distance of closest approach (d), the amount of paramagnetic centers ([C]), and the translational correlation time (τD) through Eqn (9) (Lauffer, 1987; Laurent et al., 2008):

$$R_{1out} = Y\frac{[C]}{dD}\left[7J\left(\omega_S\tau_D\right)+3J\left(\omega_I\tau_D\right)\right] \qquad (9)$$

Here, Y is a constant containing the Avogadro's number (N_A), the Plank constant, the quantum spin number, and the magnetogyric ratios (γ) of protons and paramagnetic centers, respectively J ($\omega_I\tau_D$) is the spectral density depending on the Larmor frequency of the electrons in the paramagnetic center (S) and that of the

proton nuclei (I). The translational correlation time is temperature (T) dependent as reported in Eqn (10) where η is the viscosity of the medium and k is the Boltzmann constant (Lauffer, 1987):

$$\tau_D \propto \frac{\eta d^2}{kT} \tag{10}$$

According to Eqns (9) and (10), decrement of R1out is obtained when temperature is increased due to the reduction of the temperature dependent translational correlation time values. In other words, relaxation rate reduction is achieved because temperature increment favors water molecular motion, thereby reducing the efficiency of the dipolar interactions between water and biochar surface (fast motion regime in Fig. 9) (De Pasquale et al., 2012). The second relaxation mechanism is indicated as inner-sphere relaxation mechanism and it is described by the inner-sphere longitudinal relaxation rate (R1inn = 1/T1inn).

This mechanism is related: (i) to the diffusion of water molecules to and from the and type biochar sites and (ii) to the chemical exchanges between water and biochar.

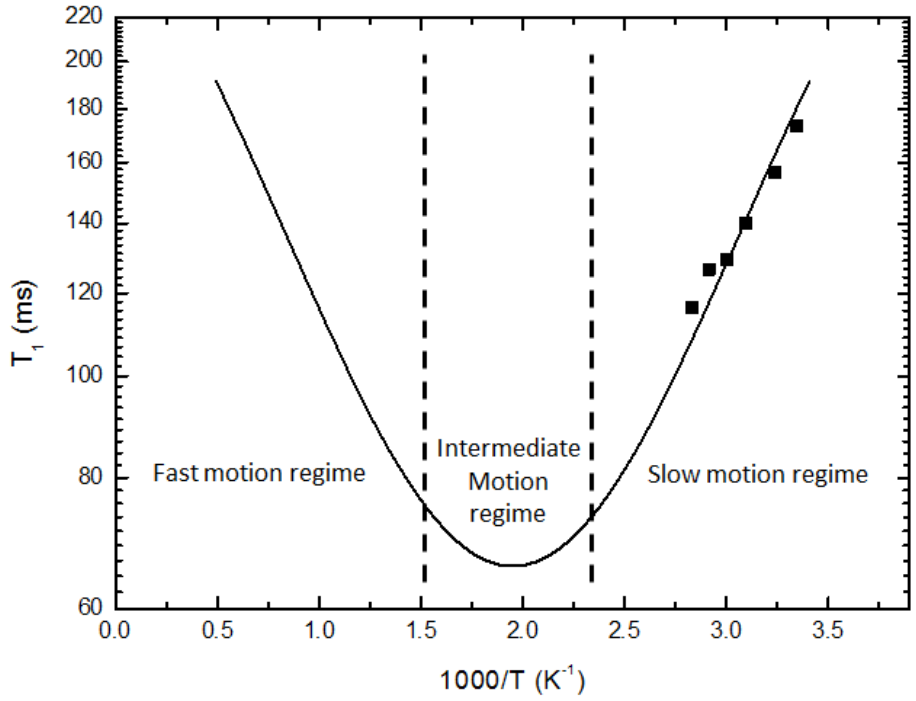

Fig. 9 Thermal variation of the longitudinal relaxation time (T1). The dots are the T1 values of the water-saturated poplar biochar measured at 39 MHz for temperature values ranging from 299 to 353 K. The continuous line is the simulation of the temperature

The inner-sphere relaxation mechanism is mediated by the H-bonds retrieved by overlaying the electron-deficient orbitals of the hydrogens in water with the orbitals containing the unpaired electrons of the inorganic and organic paramagnetic centers in biochar (Desiraju & Steiner, 1999; Belford et al., 2000). Equation (11) describes the R1inn dependency upon the molar fraction of water bound to biochar (fM), the proton longitudinal relaxation time of water coordinated to the biochar paramagnetic centers (T1M) and the exchange correlation time, τM, which measures

the mean residence time of the bound water (Korb, 2001, 2006; Alhaique et al., 2002; Caravan, 2006):

$$R_{1inn} = \frac{f_M}{T_{1M} + \tau_M} \tag{11}$$

According to Lauffer (1987), the value of T1M is described by the Solomon–Bloembergen equation (not reported here), which contains a dipolar (i.e. through space) and a scalar, or contact (i.e. through bonding- electrons), relaxation contribution. The two contributions are field dependent, therefore, they are discernible by operating with fast field cycling NMR relaxometry (Korb, 2001, 2006). Namely, scalar contribution to T1M predominates at low magnetic fields, whereas the dipolar contribution can be monitored at high magnetic fields (Lauffer, 1987). The total relaxation rate of the water-saturated biochar system is given by (Alhaique et al., 2002):

$$R_{1tot} = R_{1inn} + R_{1out} \tag{12}$$

According to the mechanisms outlined above, variable temperature fast field cycling NMR relaxometry experiments can discern whether inner- or outer-sphere relaxation contributions predominate in water-saturated biochar systems. In fact, due to the temperature dependence of the diffusional correlation time (Eqn 10), a decrease of R1tot in the entire interval of the investigated magnetic field frequencies must be observed if the outer-sphere relaxation mechanism predominates (fast

motion regime). Conversely, two different cases must be considered when R1inn prevails. In the fast motion regime (Fig. 9) where $\tau M << T1M$, the chemical exchange is fast, thereby indicating that R1tot is proportional to 1/T1M (Eqn 11). Since T1M increases as temperature is raised up because of a reduced efficiency of the dipolar and the scalar relaxation contributions, a decrease of R1tot must be obtained in the whole range of the magnetic fields spanned by FFC NMR relaxometry. When $\tau M \geq T1M$, the slow motion regime occurs (Fig. 9). In this case, R1tot depends upon the inverse of τM values (Eqn 11). Due to the increasing water mobility as temperature is raised, reduction of τM values is retrieved and displacement of the NMRD profiles toward higher R1tot values must be observed.

The black dots in Fig. 9 are the T1 values of the water-saturated poplar biochar studied here. They are measured at variable temperature at the proton Larmor frequency of 39 MHz. All the points fall in the slow motion regime region, thereby revealing that among the different mechanisms outlined above, the relaxation is dominated by the inner-sphere mechanism. This is further confirmed by the NMRD profiles reported in Fig. 10, where the curves move toward higher R1 values as temperature is increased.

According to the inner-sphere relaxation mechanism, we can infer that water molecules penetrate into the biochar pores and adhere to the surface of this carbonaceous material due to the formation of nonconventional hydrogen bonds (Desiraju & Steiner, 1999).

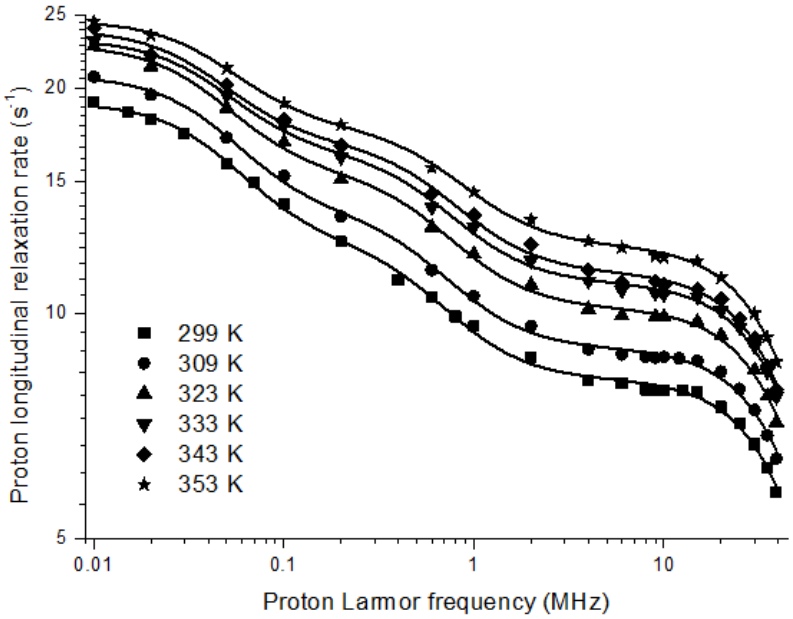

Fig. 10 NMRD profiles of water-saturated biochar at different

In our previous article (De Pasquale et al., 2012) we reported that a small amount of oxygenated functions may be present in the poplar biochar due to the partially oxidative conditions during gasification or to the storage post production conditions. However, if O–containing functions were present, they should have been revealed by high resolution solid-state NMR spectroscopy. Indeed, the spectrum of poplar biochar (not reported here) only shows an intense aromatic carbon signal centered at 126 ppm. This signal is generated by the electronic currents produced by the delocalized-electrons in extended aromatic structures or graphite -like micro-crystallites (De Pasquale et al., 2012). Moreover, the poplar biochar used in this study also contains some potentially paramagnetic centers such as Fe, Cu, and Mn (0.57, 0.30, and 0.035 g kg^{-1}, respectively, see De Pasquale et al., 2012 for details). For this reason we suggest formation of nonconventional H-bonds (Desiraju & Steiner, 1999) between water molecules and the inorganic and organic parts of

poplar biochar. According to Belford et al. (2000), such H-bonds can arise by the overlay between the electron-deficient orbitals of protons in water and the orbitals containing the unpaired electrons of the paramagnetic centers in biochar (i.e. metals and aromatic system). In his study on paramagnetic silica-based porous materials, Korb (2001, 2006) suggested that the Arrhenius graphs reporting R1 values at different temperatures and magnetic fields (Fig. 11) provide the apparent activation energy (Ea) for the proton mobility (e.g. exchange) in the surface of the porous systems.

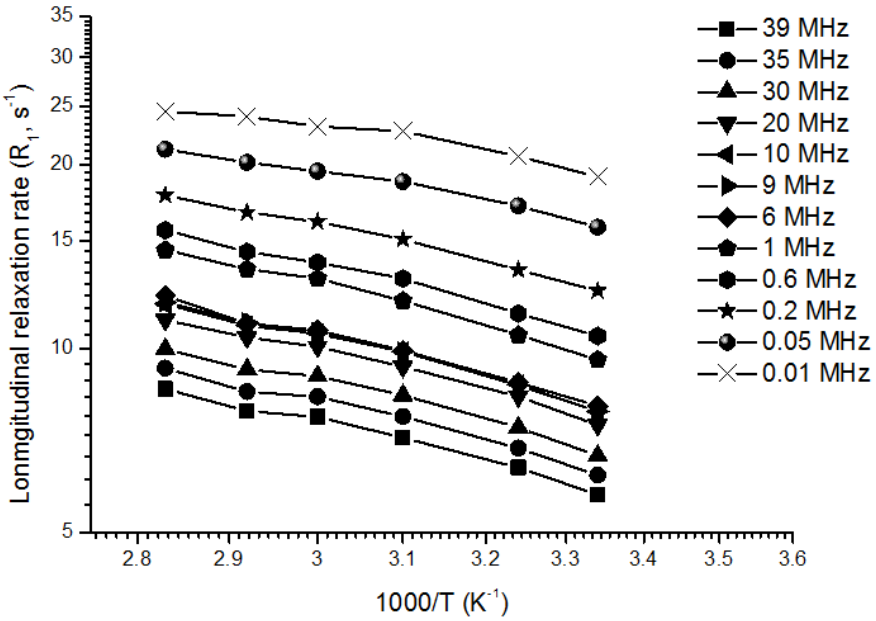

Fig. 11 Arrhenius graph of the longitudinal relaxation rate (R1)

Fitting of the datasets reported in Fig. 11 gives an apparent activation energy of 5.8 kJ mol^{-1}. According to Desiraju &Steiner (1999) this Ea value is typical for H-bonds classified as 'weak' and it is typical for water bound to -systems such as in the

alkines (Nishio et al., 1998). It must be stated that water-saturated biochar is a very complex system, therefore, a distribution of H-bonds with different energies and strengths must be conceivably hypothesized. For this reason, the Ea value of 5.8 kJ mol^{-1} must be intended as an average apparent activation energy accounting for all the possible interactions between water and poplar biochar. Application of Eqn (7) to fit the profiles in Fig. 2 provided a set of parameters (see Materials and methods) used to retrieve an average correlation time as reported in Eqn (8). The correlation time describes the random molecular motions of molecular systems in porous media (Kimmich & Anoardo, 2004; De Pasquale et al., 2012). Namely, $<\tau C>$ measures the time taken for a molecule to rotate one radian or to move a distance of the order of its own dimension (Bakhmutov, 2004). As expected, reduction of $<\tau C>$ values with temperature increment is observed (Fig. 12). In fact, as temperature is raised, the kinetics of water molecules increases, thereby allowing water to span the same volume in a shorter time. However, due to the above evidenced predominance of the inner-sphere relaxation mechanism, we suggest that the $<\tau C>$ value of the water-saturated poplar biochar corresponds to τM, which has been defined as the parameter measuring the mean residence time of the bound water. According to Bakhmutov (2004), correlation time-vs.-T curve decays exponentially following Arrhenius equation (Fig. 12) from which an activation energy (i.e. the energy needed for the molecular motion) of around 2 kJ mol^{-1} can be retrieved. Due to the impossibility to collect more data points at temperatures higher than those investigated here, the Arrhenius equation cannot be fitted properly. In fact, to obtain a good estimate of a function parameter (Ea, in the present study), it is necessary, from a mathematical

point of view, to cover the entire range of that function. In our case, only the range of temperature comprised between 299 and 353 K was analyzed.

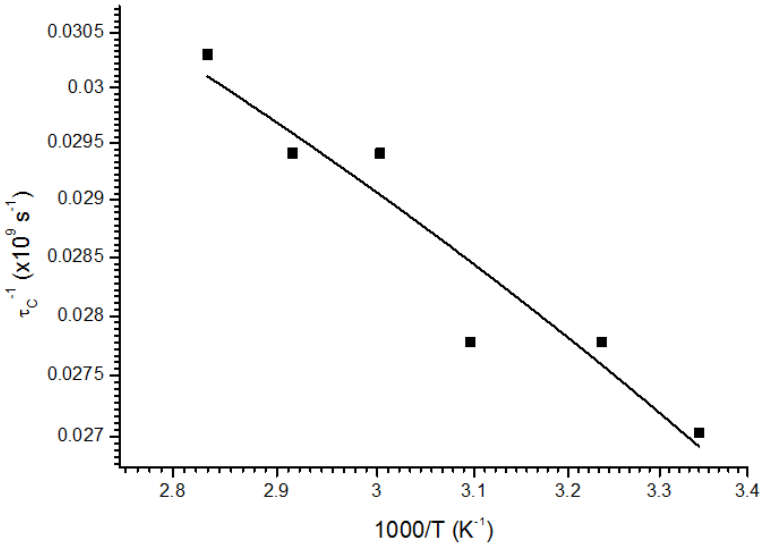

Fig. 12 Arrhenius graph for the correlation time (τ_C) of the water saturated biochar.

This range covers only the linear part of the exponential shape of the Arrhenius equation. For this reason, we argue that the two Ea values (i.e. 5.8 and 2 kJ mol^{-1}) cannot be considered different within the experimental error. Both of them ensure that water molecules are weakly bound by H-bonds either to the inorganic paramagnetic centers or to the paramagnetic hydrophobic organic part of the poplar biochar. The evaluation of the relaxometry properties of a water-saturated poplar biochar suggested that water molecules are bound to the solid carbonaceous material through nonconventional hydrogen bonds. The comprehension of the mechanisms of the water-biochar interactions is a preliminary step for the understanding of the

molecular mechanisms through which water can be drained into biochar-amended soils, thereby affecting soil physico-chemical properties. This knowledge is very crucial to address biochar agronomical and environmental uses and to allow meaningful pre application quality assessments. However, it must be also pointed out that this study deals with only one biochar from poplar residues. To validate the model of the water-biochar interactions suggested here, further studies are ongoing on biochars from different biomasses, and on those obtained at different charring temperatures.

References

Alhaique F, Bertini I, Fragai M, Carafa M, Luchinat C, Parigi G (2002) Solvent 1H NMRD study of biotinylated paramagnetic liposomes containing Gd-bis-SDA-DTPA or Gd-DMPE-DTPA. *Inorganica Chimica Acta,* **331**, 151-157.

Anoardo E, Galli G, Ferrante G (2001) Fast-Field-Cycling NMR: Applications and Instrumentation. *Applied Magnetic Resonance,* **20,** 365-404.

Bakhmutov VI (2004) Practical NMR relaxation for chemists JohnWiley & Sons Ltd, The Atrium, Southern Gate, Chichester, West Sussex PO19 8SQ, England.

Belford RL, Clarkson RB, Nilges MJ, Odintsov BM, Smirnov AI (2000) Coal and Char Studies by Advanced EMR Techniques. Final Technical Report to DOE – FETC. –Grant # DE-FG22-96PC96205. Available at: http://www.osti.gov/bridge/purl.cover.jsp?purl=/791711-1y5NHj/native/791711.pdf (accessed 14 September 2012).

Brewer CE, Unger R, Schidt-Rohr K, Brown RC (2011) Criteria to select biochars for field studies based on biochar chemical properties. *Bioenergy Research,* **4(4)**, 312–323.

Caravan P (2006) Strategies for increasing the sensitivity of gadolinium based MRI contrast agents. *Chemical Society Reviews,* **35**, 512-523.

Caravan P, Parigi G, Chasse JM, *et alii* (2007) Albumin binding, relaxivity, and water exchange kinetics of the diastereoisomers of MS-325, a gadolinium(III)-based magnetic resonance angiography contrast agent. *Inorganic Chemistry*, **46**, 6632-6639.

Clarkson RB, Odintsov BM, Ceroke PJ, Ardenkjaer-Larsen JH, Fruianu M, Belford RL (1998) Electron paramagnetic resonance and dynamic nuclear polarization of char suspensions: surface science and oxymetry. *Physics in Medicine and Biology*, **43,** 1907-1920.

De Pasquale C, Marsala V, Berns AE, Valagussa M, Pozzi A, Alonzo G, Conte P (2012) Fast field cycling NMR relaxometry characterization of biochars obtained from an industrial thermochemical process. *Journal of Soils and Sediments*, doi: 10.1007/s11368-012-0489-x.

Desiraju GR, Steiner T (1999) The weak hydrogen bond, Oxford Science Publications.

Dunn KJ, Bergman DJ, Latorraca GA (2002) Handbook of Geographic Exploration-Seismic Exploration: Nuclear Magnetic Resonance Petrophysical and Logging Applications. Elsevier Science Ltd, Oxford, UK

Ferrante G, Sykora S (2005) Technical aspects of fast field cycling. *Advances in Inorganic Chemistry,* **57,** 405-470.

Gossuin Y, Hocq A, Vuong QL, Disch S, Hermann RP, Gillis P (2008) Physico-chemical and NMR relaxometric characterization of gadolinium hydroxide and dysprosium oxide nanoparticles. *Nanotechnology*, **19,** 475102 (8pp).

Halle B, Johannesson H, Venu K (1998) Model-Free Analysis of stretched relaxation dispersions. *Journal of Magnetic Resonance*, **135**, 1-13.

Hwang L-P, Freed JH (1975) Dynamic effects of pair correlation functions on spin relaxation by translational diffusion in liquids. *J. Chem. Phys*, **63,** 4017-4023.

Kimmich R, Anoardo E (2004) Field-cycling NMR relaxometry. *Progress Nuclear Magnetic Resonance Spectroscopy*, **44,** 257–320.

Korb J-P (2001) Surface dynamics of liquids in porous media. *Magnetic Resonance Imaging*, **19,** 363-368.

Korb J-P (2006) Surface diffusion of liquids in disordered nanopores and materials: a field cycling relaxometry approach. In: *Fluid transport in*

nanoporous materials (eds WC Conner and J Fraissard) pp. 415-437. Springer, The Netherlands.

Laudicina VA, De Pasquale C, Conte P, Badalucco L, Alonzo G, Palazzolo E (2012) Effects of afforestation with four unmixed plant species on the soil–water interactions in a semiarid Mediterranean region (Sicily, Italy). *Journal of Soils and Sediments,* doi 10.1007/s11368-012-0522-0.

Lauffer RB (1987) Paramagnetic metal complexes as water proton relaxation agents for NMR imaging: theory and design. *Chemical Reviews.* **87**, 901-927.

Laurent S, Forge D, Port M, Roch A, Robic C, Elst LV, Muller RN (2008) Magnetic ion oxide nanoparticles: synthesis, stabilization, vectorization, physicochemical characterizations, and biological applications. *Chemical Reviews,* **108,** 2064-2110.

Lehmann J, Joseph S (2009) Biochar for environmental management: an introduction. In: *Biochar for environmental management: science and technology* (eds Lehmann J, Joseph S) pp. 1–13. Earthscan, London.

Morozova-Roche LA, Jones JA, Noppe W, Dobson CM (1999) Independent Nucleation and Heterogeneous Assembly of Structure during Folding of Equine Lysozyme. Journal *of Molecular Biology*, **289**, 1055-1073.

Nishio M, Hirota M, Umezawa Y (1998) The CH/π interaction: evidence, nature, and consequence. Wiley-VCH NY, USA.

Strijkers GJ, Mulder WJM, van Heeswijk RB, Frederik PM, Bomans P, Magusin PCMM, Nicolay K (2005) Relaxivity liposomal paramagnetic MRI contrast agents. *Magnetic Resonance Materials in Physics, Biology and Medicine,* **18**, 186-192.

Warnock DD, Lehmann J, Kuyper TW, Rilling MC (2007) Mycorrhizal responses to biochar in soil—concepts and mechanisms. *Plant and Soil,* **300**, 9–20.

7. NATURE OF SURFACE INTERACTIONS AT THE INTERFACE OF TWO WATER-SATURATED COMMERCIAL TiO_2 POLYMORPHS

Pellegrino Conte, Vittorio Loddo, Claudio De Pasquale, Valentina Marsala, Giuseppe Alonzo, Leonardo Palmisano

dx.doi.org/10.1021/jp400298m | J. Phys. Chem. C

7.1 Abstract

Two commercial TiO_2 samples, a 100% anatase and a 100% rutile were used for the fast field cycling NMR experiments. The results showed a different behavior between the different samples. In particular, water molecules were unbonded to the solid surface for the rutile sample, whereas they appeared to chemically interact to the surface trough H-bond formation with the anatase sample The above findings accord with the generally lower activity of rutile with respect to anatase reported in literature for photocatalytic oxidation reactions in water. The difficulty of water to interact with rutile surface, indeed, could hinder the formation of OH radicals, which are the most important oxidant species.

Keywords: fast field cycling relaxometry; NMRD; rutile; anatase; H-bonds; surface interactions

7.2 Introduction

Titanium dioxide either powdered or in the form of thin films supported on different kinds of materials is widely applied in photocatalysis for pollutant abatement (Schiavello, 1988; Serpone and Pelizzetti, 1989; Ollis and El Ekabi, 1993; Schiavello, 1997; Augugliaro et al., 2010), partial oxidation or reduction of organic and inorganic molecules in chemical syntheses (Palmisano et al., 2007; 2010; Augugliaro et al., 2012), in solar cells for the production of hydrogen, as a gas sensor, as a white pigment such as in paints and cosmetics, as an optical coating, as a corrosion-protective coating, and in many electric devices (Diebold, 2003). Titanium dioxide plays also a very important role in biocompatibility for bone implants and in the realization of electronic components such as those applied for nuclear magnetic resonance instruments (Diebold, 2003).

All the peculiarities of titanium dioxide depend on the surface characteristics of such material (Sclafani et al., 1990a, b) which, in turn, are affected by the preparation methods applied for its achievement (Augugliaro et al., 2008, 2010). In fact, it is well recognized that polymorphism, cristallinity degree, and amount of surface defects are all dependent on the nature of the parent material, and the temperature and pressure achieved during TiO_2 preparation (Schiavello, 1988, 1997; Diebold, 2003; Augugliaro et al., 2008, 2010; Yurdakal et al., 2008).

Because of its properties, titanium dioxide is widely applied in green chemistry where water is used as a “green” solvent due to its null or negligible environmental impact as compared with the traditional solvents employed in organic and inorganic syntheses (Henderson, 2002). For this reason, studies concerning the way how water binds to TiO_2 surface are of paramount importance (Henderson,

2002; Diebold, 2003). In fact, as an example, TiO_2 selectivity for organic molecules appears to be affected by wet adsorption conditions (Polunina et al., 1999; Yurdakal et al., 2008), whereas the efficaciousness of the red-ox transformations on titanium dioxide catalysts strongly depends on the way how water molecules dissociate on the TiO_2 solid surface (Diebold, 2003).

Many papers, mostly reviewed in Henderson (2002) and Diebold (2003), deal with the interactions of water on the surface of pure crystalline TiO_2 polymorphs. The majority of such papers concern mainly theoretical evaluation of water-TiO_2 interactions. Only a few results were experimentally retrieved primarily on the crystalline forms of rutile TiO_2 (indicated simply as rutile from now-on) by applying, as an example, ultraviolet photoemission spectroscopy, electron energy loss spectroscopy, Auger electron spectroscopy, X-ray photoelectron spectroscopy and temperature programmed desorption investigations (Diebold, 2003). The interactions between water and anatase TiO_2 (that will be further indicated only as anatase) have been, up to now, investigated only theoretically (Diebold, 2003). Just a few X-ray photoelectron spectroscopy experiments have been conducted on water-anatase interactions due to the lower importance of such polymorph as compared to rutile (Diebold, 2003). To the best of our knowledge, the interaction of water with the surface of the commercial forms of rutile and anatase has not yet been investigated.This investigation is very important due to the prevalence of such materials on the market and to explain the reason why commercial rutile appears less effective than commercial anatase (Yurdakal et al., 2008). The aim of the present article is, then, the evaluation of the nature of the interactions between water

and commercial rutile and anatase by using fast field cycling (FFC) NMR relaxometry whose peculiarities are reported in the Supporting Information.

7.3 Materials and Methods

7.3.1 Samples.

Rutile and anatase were purchased by Sigma-Aldrich (Milan, Italy) and Merck (Milan, Italy), respectively. Their surface area (SA) was measured by the dynamic Brunauer–Emmett–Teller (BET) method using a Micromeritics Flowsorb 2309 apparatus (Dunstable, UK) with nitrogen as the adsorbate. SA of rutile resulted 2.5 $m^2 \cdot g^{-1}$, whereas that of anatase was 10 $m^2 \cdot g^{-1}$.

7.3.2 Fast field cycling (FFC) NMR experiments.

552.0 mg of rutile and 512.9 mg of anatase were suspended in 3.0206 g and 3.0081 g of deionized water, respectively. The suspensions were allowed to sediment overnight prior to the relaxometry investigations. The samples were put in the probe of a Stelar Smartracer fast-field-cycling relaxometer (Stelar s.r.l., Mede, PV–Italy) and analyzed at 298, 313, 333, 343, and 353 K.

The basic theory about FFC NMR relaxometry is reported in Kimmich and Anoardo (2004) and Ferrante and Sykora (2005). The details on the FFC NMR sequence used in the present study have been already published (De Pasquale et al. 2012). They are also reported in the Supporting Information together with the experimental details that have already been reported in Conte et al. (2012). The only differences between the parameters used in the present study and those reported in Conte et al. (2012) concern the proton Larmor frequencies (PLFs) used to perform the analyses. Here the PLFs of the relaxing magnetic field (B_{RLX}) were varied from 0.01 up to 10 MHz, the proton Larmor frequency of the polarization field (B_{POL}) for

the pre-polarized sequence (De Pasquale et al., 2012) was set at 10 MHz, whereas the PLF for free induction decay acquisition (B_{ACQ}, see Supporting Information) was set at 7.2 MHz. The nuclear magnetic resonance dispersion (NMRD) curves, obtained by measuring the longitudinal relaxation rates ($R_1=1/T_1$) at each B_{RLX} (see Supporting Information), provide information about the spectrum of the reorientational and diffusional molecular dynamics (Kimmich and Anoardo, 2004). All measurements were repeated twice. The error on each R1 value was 10%. Figure 1 reports the relaxation rate versus PLFs (i.e., NMRD profiles) ateach temperature with error bars on R1.

7.4 Results

Fig. 13 reports the NMRD profiles of rutile and anatase TiO_2 polymorphs at different temperatures. All profiles showed the classical stretched Lorentzian shapes (Kimmich and Anoardo, 2004). In particular, the profiles retrieved for rutile were at slower R_1 values (Fig. 13A) than those acquired for anatase (Fig. 13B).

The temperature dependence of the NMRD profiles for rutile and anatase revealed opposite trends. In fact, whereas rutile profiles showed R_1 values decreasing with temperature enhancement (Fig. 13A), anatase profiles revealed a direct proportionality between proton longitudinal relaxation rate values and temperature (Fig. 13B). In addition, as temperature overcome 343 K, the NMRD profiles of anatase appeared to cross those obtained at lower temperatures (from 298 to 333 K) for the same water-saturated material as the PLF became lower than 0.1 MHz (Fig.14 B).

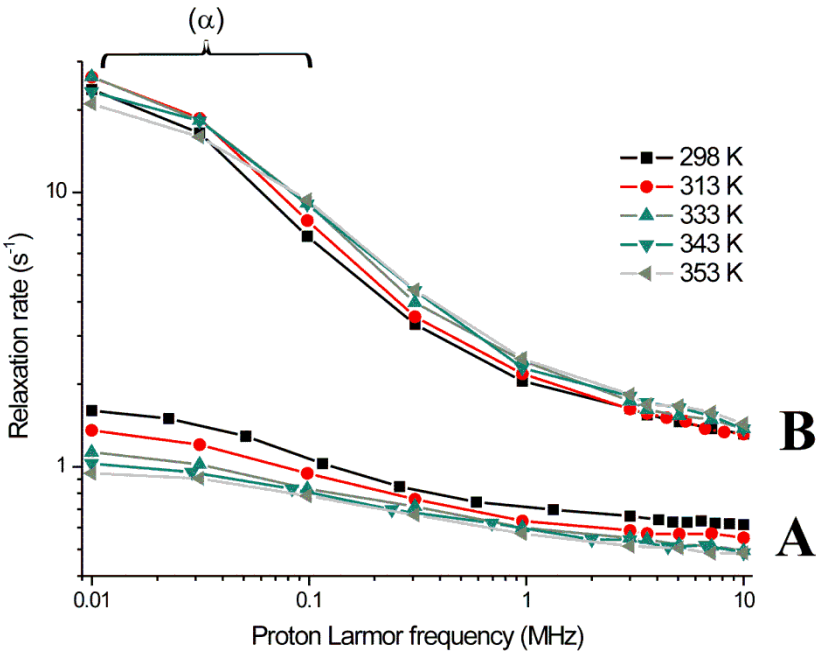

Fig. 13 NMRD profiles at different temperatures of A. rutile and B. anatase. (α) is the proton Larmor frequency region of the applied magnetic field where the NMRD profiles of anatase at 343 and 353 K cross those at the lowest temperatures (298, 313 and 333 K).

7.5 Discussion

Water dynamics on the surface of porous media is related to SA values. The latter, in turn, depends on pore sizes (Schure et al., 1985). In fact, the smaller the pore sizes, the larger is the SA value. Conversely, SA reduction is achieved when the sizes of the pores increase. As water molecules flow through larger sized pores, their motion occurs at a frequency that is broader than that of water molecules constrained in smaller sized pores. For this reason, quickly moving water cannot efficaciously interact with either the neighboring molecules or with the molecular sites on the surface at the liquid-solid interface. As a consequence, intermolecular dipolar interactions are weakened and a reduction of the proton longitudinal

relaxation rate (shorter R_1 values) can be observed as compared to the R_1 values for slowly moving or immobilized water systems (Bakhmutov, 2004).

In the present study, SAs of rutile and anatase resulted 2.5 $m^2 \cdot g^{-1}$ and 10 $m^2 \cdot g^{-1}$, respectively. It is, then, expected that $R_{1(rutile)} < R_{1(anatase)}$. Fig. 13 confirms such expectation. In fact, all the NMRD profiles achieved for the water saturated rutile are placed at shorter R_1 values (Fig. 13A) compared to the profiles of the water saturated anatase (Fig. 13B).

The feasibility of the proposed water molecular mobility mechanism was also investigated by variable temperature experiments. In fact, it is well recognized that the time spent by water on the surface of porous media decreases as temperature is increased (Kimmich and Anoardo, 2004). As water mobility is increased because of temperature enhancement, dipolar interactions at the solid-liquid interface are weakened. This leads to longer time for proton relaxation (shorter R_1 values) (Bakhmutov, 2004). A close look at the temperature dependence of the NMR profiles in Fig. 13, reveals that the aforementioned expectation (i.e. NMRD profiles moving towards shorter R_1 values with temperature enhancement) was achieved only for the water molecules saturating rutile (Fig. 13A). Conversely, water-saturating anatase provided NMRD profiles that were not only translated towards longer R_1 values but also changed in slope. In fact, the NMRD curves obtained at 343 and 353 K crossed those retrieved at the lowest temperatures (Figure 1B). Clearly, pore size cannot be the only factor affecting water dynamics on the surface of the two titanium dioxide polymorphs.

Lauffer (1987), Korb (2001), Kimmich and Anoardo (2004), Korb and Bryant (2005) and Laurent et al. (2008) reported that the correct chemical-physical

approach to understand the molecular dynamics of a fluid on a solid surface must be based on two possible mechanisms. From the one side, water diffuses by the porous medium surface, from a distance "d", usually indicated as distance of closest approach, and infinity (Hwang and Freed, 1975). This diffusion occurs when non-chemically interacting water is replaced by another similar molecule belonging to the bulk water system (Fig. 14A). The time spent by water on the solid surface can be affected by the formation of H-bonds due to the presence of either hydrogen acceptors or hydrogen donors on the outer boundary (Conte et al., 2012). Following H-bond formation, hydrogen atoms can also be subjected to rapid exchanges between water molecules and the porous surfaces as depicted in Fig. 14B. The mathematics of the aforementioned mechanism is described by equation [13] (Lauffer, 1987; Laurent et al., 2008):

$$R_1 = Y\frac{[C]}{dD}\left[7J\left(\omega_S\tau_D\right)+3J\left(\omega_I\tau_D\right)\right]+\frac{f_M}{T_{1M}+\tau_M} \qquad (13)$$

Here, [C] is the amount of paramagnetic centers, *d* is the distance of the closest approach, D is the diffusion coefficient and Y is a constant. The latter accounts for the Avogadro's number (N_A), the Plank constant, the quantum spin number and the magnetogyric ratios (γ) of the observed nuclei (^1H) and the paramagnetic centers. $J\left(\omega_i\tau_D\right)$ is the spectral density depending on the Larmor frequency of the electrons in paramagnetic centers (S) and that of proton nuclei (I). f_M represents the molar fraction of water chemically bound to the porous system (BW), T_{1M} is the proton longitudinal relaxation time of the chemically bound water,

and τ_M is the exchange correlation time, which measures the mean residence time of the bound water (Conte et al., 2012).

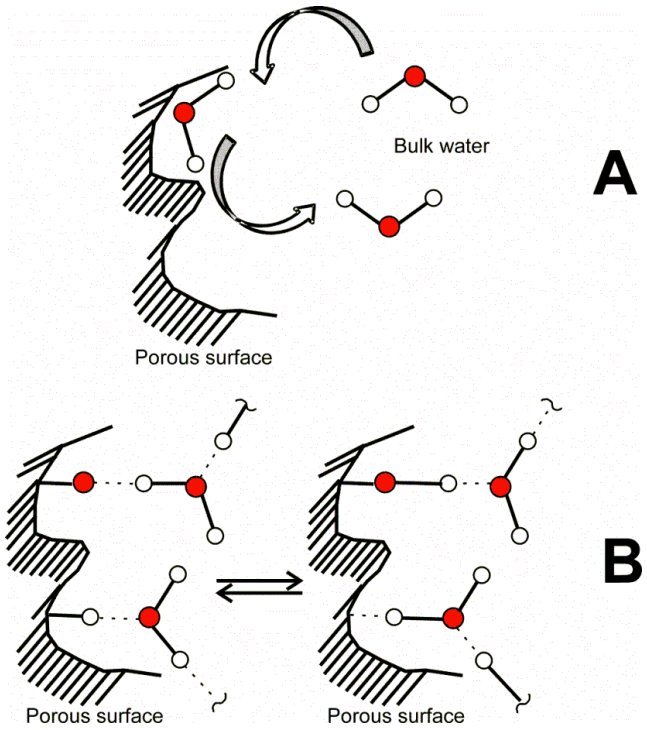

Fig. 14. Mechanisms of water dynamics on porous media surfaces. A. Diffusivity of bulk water through surface porous. B. Exchanges of hydrogen between water and porous surface as mediated by H-bond interactions (dashed lines). The red dots are the oxygen atoms, while the white ones represent the hydrogen atoms.

The first term on the right side of equation [13] describes the diffusional motion of water as depicted in Fig. 14A, whereas the second term represents the water motion mediated by hydrogen bonds, as represented in Fig. 14B. Because of the absence of paramagnetic centers in the two TiO_2 polymorphs used for the present study, the contribution of the first term in equation [13] can be neglected. For this reason the longitudinal relaxation rate of the water saturated TiO_2 polymorphs

depends on BW amount, on BW proton longitudinal relaxation time and on the exchange correlation time.

Two different cases must be considered. When $\tau_M \ll T_{1M}$, fast motion regime occurs (Conte et al., 2012). Under this condition, the proton longitudinal relaxation rate is proportional to $1/T_{1M}$. In particular, the proton exchange between water and TiO_2 surface occurs as depicted in Fig. 14A, thereby allowing the consideration that water is not chemically retained on the titanium dioxide surface. According to Lauffer (1987), the proton longitudinal relaxation time value of the unbound water decreases as temperature is increased. In fact, T_{1M} contains a dipolar (i.e. through space) and a scalar, or contact (i.e. through bonding-electrons), relaxation contribution (Lauffer, 1987). Both of them reveal a reduced efficiency as temperature is increased. For this reason, reduction of R_1 values in the whole range spanned by FFC NMR relaxometry can be measured (Bakhmutov, 2004).

As $\tau_M \gg T_{1M}$, slow motion regime occurs (Conte et al., 2012). In this case the proton longitudinal relaxation rate depends upon $1/\tau_M$ and water appears bound to the porous medium surface due to formation of H-bonds (Fig. 14B). Because of the inverse relationship between correlation time and temperature (Bakhmutov, 2004), an increase of R_1 values is achieved as temperature is enhanced.

On the basis of the mechanism founded on equ 13, we can conclude that water molecules interact chemically to the surface of anatase through H-bond formation. Conversely, water is virtually unbound to the surface of rutile.

It is worth noting that the lack of chemical interactions between water and rutile found by FFC NMR relaxometry accords with its generally low photochemical activity (Palmisano et al., 2007; Sclafani et al.,1990; Gupta et al., 2011). In fact, low

photoactivity of commercial rutile has been observed when it is used for both photomineralization and selective photooxidation reactions in water .

The mechanism of the photocatalytic oxidation reactions foresees formation of ·OH radicals that are believed to be responsible for the primary oxidant attack to the substrate. The interaction between adsorbed water and TiO_2 surface plays the major role to produce the oxidant species according to the following steps:

$$TiO_2 \xrightarrow{h\nu} TiO_2(e^-_{CB}, h^+_{VB}) \quad (14)$$

$$H_2O + h^+_{VB} \xrightarrow{TiO_2} {}^{\cdot}OH + H^+ \quad (15)$$

$${}^{\cdot}OH + substrate \rightarrow oxidised..products \quad (16)$$

$${}^{\cdot}oxidised...products \xrightarrow{{}^{\cdot}OH} \xrightarrow{{}^{\cdot}OH} H_2O + CO_2 + inorganic...species \quad (17)$$

Consequently, the absence of chemical interactions between H_2O and the surface of rutile, as highlighted by NMRD results, strongly suggests that the formation of ·OH radicals from H_2O, according to equation 15, is highly improbable. However, it must be stated that high levels of rutile photoactivity, for both photomineralization and selective photo-oxidation reactions in water, can be attained when this catalyst is prepared under milder experimental conditions (Sclafani et al.,1990 Yurdakal et al., 2008).

Although our results accord with some literature data, (Palmisano et al.,2007; Sclafani et al.,1990; Gupta et al.,2011) they appear to discord with those provided in Beck et al.,(1986) Jug et al., (2005) and Erdogan et al., (2005). In fact, those authors reported that water can interact with rutile surface mainly in its dissociate form

(hydroxylated rutile). The discrepancy between the NMRD results reported here and those aforementioned can be accounted for in two different ways. From the one hand, Beck et al.(1986) used two different rutile materials in their experiments. One of the rutile forms showed a SA of 11 m^2 g^{-1}, whereas the second had a SA of 30 $m^2 \cdot g^{-1}$. As reported in the Materials and Methods, we used a rutile having a SA of 2.5 $m^2 \cdot g^{-1}$. It is known that the amount of hydroxylated TiO2 sites increases as SA becomes larger (Sclafani et al., 1990). For this reason, the number of H bonds that water can form with rutile is directly proportional to the SA value. Because of the low number of H bonds conceivably present in the rutile used in the present study, it is possible to argue that FFC NMR relaxometry wasunable to reveal the interactions between water and the rutile surface. Jug et al. (2005) and Erdogan et al. (2011) reported about computational calculations on cyclic cluster models of rutile pure crystals to achieve information about the energy involved in the different ways water can interact with rutile. For this reason, a comparison between our results and those described in Jug et al. (2005) and Erdogan et al. (2011) is not feasible.

At the largest temperature values (343 and 353 K) the NMRD profiles of anatase crossed those retrieved at temperatures comprised in the range 298-333 K as the PLF of the applied magnetic field became lower than 0.1 MHz (Fig. 13B). A possible explanation of such a behavior is related to the interruption of the diffusive processes at the solid-liquid interface by the chemical exchanges with the bulk water (Korb, 2001).

The findings reported on anatase in the present study appear to confirm the theoretical calculations provided by Vittadini et al. (1998). In fact, these authors reported that water is molecularly adsorbed on the surface of anatase through

formation of hydrogen bondings. In addition, they also reported that temperature enhancement favors water dissociation and hydroxylation of anatase surface. However, we do think that the anomalous behavior at high temperatures reported in Fig. 13B cannot be attributed to water dissociation and surface hydroxylation. As suggested by Korb (2001), it can be due to the alteration of the diffusive processes as a consequence of the chemical exchanges becoming important as $T \geq 343$ K. The temperature needed for water dissociation on TiO_2 surface must be at least >400 K (Beck et al., 1986).

7.6 Conclusions

The present article shows for the first time the nature of the interactions between water and the surface of two commercially available titanium dioxide polymorphs. In particular, a low SA rutile produced by Sigma-Aldrich was compared with a high SA anatase produced by Merck. Results indicated that the low specific SA in rutile prevented formation of chemical interactions with water.

The above findings justify the low photoactivity observed when rutile samples, prepared at high temperatures such as the Sigma-Aldrich one, are used for both photomineralization and selective photooxidation reactions in water.

Conversely, hydrogen bonds between water and the surface of anatase sample have been hypothesized to explain the slow motion regime revealed by FFC NMR relaxometry experiments. The presence of H-bonds not only explained the better anatase photoreactivity as compared with the rutile above, but also confirmed literature results that have been only theoretically obtained.

To the best of our knowledge this is the first time an NMR technique has been applied to distinguish the different surface properties of commercially available TiO_2 polymorphs. The potentiality showed by fast field cycling NMR relaxometry in revealing differences between rutile and anatase will be further applied to investigate the effects of surface areas and cristallinity degree on water motion regimes.

References

Augugliaro V, Caronna T, Loddo V, Marcì G, Palmisano G, Palmisano L, Yurdakal S (2008) Oxidation of Aromatic Alcohols in Irradiated Aqueous Suspensions of Commercial and Home-Prepared Rutile TiO_2: A Selectivity Study, Chemistry A European Journal 14: 4640-4646

Augugliaro V, Loddo V, Pagliaro M, Palmisano G, Palmisano L (2010) Clean by light irradiation: Practical application of supported TiO_2, RCS Publishing, Cambridge (UK)

Augugliaro V, Bellardita M, Loddo V, Palmisano G, Palmisano L, Yurdakal S (2012) Overview on oxidation mechanisms of organic compounds by TiO_2 in heterogeneous photocatalysis, 13: 224-245

Bakhmutov VI (2004) Practical NMR relaxation for chemists. Wiley, Chichester

Beck DD, White JM, Ratcliffe CT (1986) Catalytic reduction of CO with hydrogen sulphide. 2. Adsorption of H_2O and H_2S on anatase and rutile Journal of Physical Chemistry 90: 3123-3131

Conte P, Marsala V, De Pasquale C, Bubici S, Valagussa M, Pozzi A, Alonzo G (2012) Nature of water-biochar interface interactions. GCB Bioenergy, doi: 10.1111/gcbb.12009

De Pasquale C, Marsala V, Berns AE, Valagussa M, Pozzi A, Alonzo G, Conte P (2012) Fast field cycling NMR relaxometry characterization of biochars obtained from an industrial thermochemical process. Journal of Soils and Sediments, 12:1211–1221

Diebold U (2003) The surface science of titanium dioxide. Surface Science Reports. 48: 53-229

Erdogan R, Fellah MF, Onal I (2011) An ONIOM and DFT study of water adsorption on rutile TiO_2 (110) cluster International Journal of Quantum Chemistry 111: 174-181

Ferrante G, Sykora S (2005) Technical aspects of fast field cycling. Adv Inorg Chem 57:405-470

Henderson MA (2002) The interaction of water with solid surfaces: fundamental aspects revisited. Surface Science Reports. 46: 1-308

Hwang L-P, Freed JH (1975) Dynamic effects of pair correlation functions on spin relaxation by translational diffusion in liquids. J. Chem. Phys, 63, 4017-4023

Jug K, Nair NN, Bredow T (2005) Molecular dynamics of water adsorption on rutile surfaces. Surface Science 590: 9-20

Kimmich R, Anoardo E (2004) Field-cycling NMR relaxometry. Prog Nucl Magn Reson Spectrosc 44: 257–320

Korb J-P (2001) Surface dynamics of liquids in porous media. Magnetic Resonance Imaging 19: 363-368

Korb J-P, Bryant RG (2005) Magnetic relaxation dispersion in porous and dynamically heterogeneous materials. Advances in Inorganic Chemistry 57:293-326

Lauffer RB (1987) Paramagnetic metal complexes as water proton relaxation agents for NMR imaging: theory and design. Chemical Reviews. 87, 901-927.

Laurent S, Forge D, Port M, Roch A, Robic C, Elst LV, Muller RN (2008) Magnetic ion oxide nanoparticles: synthesis, stabilization, vectorization, physicochemical characterizations, and biological applications. Chemical Reviews, 108, 2064-2110

Luchinat C, Parigi G (2008) Nuclear Relaxometry Helps Designing Systems for Solution DNP on Proteins. Appl Magn Reson 34, 379-392

Ollis DF, El-Ekabi H (Eds.) (1993) Photocatalytic Purification and Treatment of Water and Air, Elsevier Science Publ., New York

Palmisano G, Yurdakal S, Augugliaro V, Loddo V, Palmisano L (2007) Photocatalytic Selective Oxidation of 4-Methoxybenzyl Alcohol to Aldehyde in Aqueous Suspension of Home-Prepared TiO_2 Catalyst, Adv. Synth. Catal., 349; 964-970

Palmisano G, García-López E, Marcì G, Loddo V, Yurdakal S, Augugliaro V, Palmisano L (2010) Advances in Selective Conversion by Heterogeneous Photocatalysis, Chem. Commun., 46: 7074-7089

Polunina IA, Isirikyan AA, Polounine KE, Mikhailova SS (1999) Water influence on the surfactant adsorption on TiO_2. Colloids and Surfaces A: Physicochemical and Engineering Aspects 160: 141–146

Sclafani A, Palmisano L, Schiavello M (1990a) Influence on the preparation methods on the photocatalytic activity of phenol in aqueous dispersion. J. Phys. Chem., 94, 829-832.

Sclafani A, Palmisano L, Davì E (1990b) Photocatalytic degradation of phenol by TiO2 aqueous dispersions: rutile and anatase activity. New J. Chem., 14, 265-268.

Schiavello M (Ed.) (1988) Photocatalysis and Environment Trends and Applications, Kluwer Academic Pu., Dordrecht, (NL).

Schiavello M (Ed.) (1997) Heterogeneous Photocatalysis, Wiley Series in Photoscience and Photoengineering, vol. 3, J. Wiley & Sons., Chichester, (UK).

Schure MR, Soltys PA, Natusch DFS, Mauney T (1985) Surface area and porosity of coal fly ash. Environmental Science and Technology 19, 82-86

Serpone N, Pelizzetti E (Eds.) (1989) Photocatalysis, Fundamentals and Applications, J. Wiley & Sons, Chichester (UK)

Vittadini A, Selloni A, Rotzinger FP, Grätzel M (1998) Structure and energetics of water adsorbed at TiO_2 anatase (101) and (001) surfaces. Physical Review Letters 14: 2954-2957.

Yurdakal S, Palmisano G, Loddo V, Alagöz O, Augugliaro V, Palmisano L (2009) Selective Photocatalytic Oxidation of 4-Substituted Aromatic Alcohols in Water with Rutile TiO_2 Prepared at Room Temperature. Green Chemistry 11, 510-516.

8 Conclusion

Energy request to satisfy human activity is growing but at the same time conventional fossil fuel exploitation is not sustainable for environment.

Biochar production and application are actually very important topics. Several authors, in fact, demonstrated the efficiency of biomass conversion into biochar, in therms of energy production. Positive effect of biochar on soil properties and its positive influence on C-Cycle, determining a reduction of CO_2 concentration in atmosphere.

Discussion on the potential biomass to use in a thermo-chemical treatment is open, in fact the conversion of different kind of biomass is an opportunity in several sector. Thermo-chemical conversion of wastes or residues to biochar offers an attractive option for minimising waste product and reducing costly transport of essentially wet biomasses (Van Zwieten et al., 2010).

Numerous benefits derived from biochar, but, more research activity is necessary to complete the description of biochar influence as soil amendment in different soil-climate conditions and with different crops.

Biochars have widely varying properties that escape characterization using simple parameters (Xu et al.,2013).

Our study have confirmed different behaviour of biochar derived from different bioamasses. Water interaction on biochar surface is strongly influenced by pore size dimension as well as the presence of inorganic paramagnetic centers or paramagnetic hydrophobic organic part on biochar surface. This interaction is very complex, obtained results suggested that water molecules are bound to the solid carbonaceous material through nonconventional hydrogen bonds.

These evaluations add important information to our knowledge on biochar properties, however further studies are necessary to validate the suggested model.

Nowadays some international organisation have started to establish guidelines to ensure safety of biochar application into soil and to direct more homogeneous production. In particular EBC (European Biochar Foundation) and IBI (International biochar initiative) have selected criteria for gaining the biochar certificate. The certificate has been developed to become a voluntary standard, it is important to note in fact that an adequate policy is missing.

Biochar's carbon content, molar H/C ratio as indicator of biochar stability, O/C ratio, the biochar nutrient content with regard to N, P, K, Mg and Ca, thresholds for heavy metals, metalloids and other elements, biochar pH, bulk density, water content, specific surface area and water holding capacity, PAHs content, PCBs, dioxins are selected as parameters to determine not only biochar's quality, but even the sustainability of its production and a positive carbon footprint.

References:

Van Zwieten L., Kimber S., Morris S., Chan K. Y. Downie A., Rust J., Joseph S., Cowie A. Effects of biochar from slow pyrolysis of papermill waste on agronomic performance and soil fertility Plant Soil (2010) 327:235–246 DOI 10.1007/s11104-009-0050-x

G. Xu, L.L. Wei, J.N. Sun, H.B. Shao, S.X What is more important for enhancing nutrient bioavailability with biochar application into a sandy soil: Direct or indirect mechanism?. Chang Ecological Engineering 52 (2013) 119–124

http://www.european-biochar.org/en

http://www.biochar-international.org/biochar